Defining Coastal Antarctic polynyas in satellite observations and climate model output to support ecological climate change research

Laura Landrum[1], Alice K. DuVivier[1], Marika M. Holland[1], Kristen Krumhardt[1], Zephyr Sylvester[2]

[1]NSF National Center for Atmospheric Research, Boulder, CO, USA
[2]INSTAAR, University of Colorado, Boulder, CO, USA

Correspondence to: Laura Landrum (landrum@ucar.edu)

Abstract. Antarctic coastal polynyas are key components of Antarctic marine ecosystems, influencing light and nutrient availability and open water access for marine predators. Thus, changes in the physical characteristics of polynyas can influence how these ecosystems respond to a changing climate. Here, we explore how to identify polynyas using satellite and Earth System Model data, and we assess the impacts of using different polynya-identification metrics and thresholds (sea ice concentration or thickness). Our results show optimal metrics for coastal polynya definition will depend on both the data resolution, as well as the season and region of interest. Temporal resolution (daily vs monthly) has an impact on polynya identification in specific regions and seasons and but has no significant impact on integrated hemispheric coastal polynya area. Our results highlight the importance of identifying polynyas on grids of the same type and resolution when comparing polynyas from different data products. We find that sea ice thickness is more suitable for identifying polynyas in model data in winter months in contrast to spring months when both sea ice thickness and concentration may be suitable metrics. The Community Earth System Model Version 2 (CESM2) identifies similar integrated Antarctic coastal polynya areas and locations as satellite based sea ice data, although polynyas identified in the CESM2 tend to be larger and fewer in number than those identified in the satellite products particularly in the winter. We then use the CESM2 to investigate ecosystem function within polynyas and find that there is enhanced phytoplankton productivity in modeled polynya features in both hindcast and fully coupled simulations. Springtime polynyas remain an important control on Antarctic productivity under future climate change, although the relative role of polynyas decreases as polynyas diminish and phytoplankton productivity outside of polynyas increases as sea ice cover decreases.

1 Introduction

Sea ice is an important component of the Antarctic physical Earth system and has a strong influence on ecosystems. Pan-Antarctic sea ice changes have been exceptionally variable in recent years, and regional trends can also differ substantially in sign and magnitude (e.g., Fogt et al., 2023; Parkinson 2019; Purrich & Doddridge, 2023; Raphael & Handcock, 2022; Turner et al., 2017; Turner et al., 2022). Yet, assessing pan-Antarctic or regional ice area trends does not address changes in important Antarctic sea ice features, specifically coastal polynyas. Polynyas are regions of reduced sea ice concentration surrounded by

higher sea ice concentrations and/or coastline, and both open water ("sensible heat") and coastal ("latent heat") polynyas are found in the Antarctic sea ice zone. Open water polynyas are created when relatively warm ocean water upwells to the surface thermodynamically melting sea ice. Coastal polynyas are driven by cold downslope winds off the Antarctic continent that mechanically push sea ice away from the coast leaving open water that can rapidly freeze into more sea ice.

Coastal polynyas occupy only a small area within the Southern Hemisphere sea ice zone yet play an outsized role in Antarctic sea ice production, deep water formation, global thermohaline circulation, carbon sequestration, and biological activity. As regions of lower sea ice concentration and thinner sea ice, polynyas are the first oceanic regions exposed to light in the Antarctic spring. As a result, polynyas show enhanced production within the Antarctic sea ice zone, where phytoplankton growth tends to be limited by light (Arrigo and van Dijken, 2003) and spring phytoplankton blooms within polynyas are frequently synchronized with light availability (e.g. Li et al., 2016). Polynyas also provide Antarctic predators (e.g., penguins, seals) both open water access and augmented prey resources, with ephemeral polynyas being of particular importance for Emperor penguins (Labrousse et al., 2019).

How Antarctic marine ecosystems respond to a changing climate will be determined, at least in part, by changes in the sea icescape, including the size, location and timing of coastal polynyas. Defining polynyas as areas of relatively open water surrounded by sea ice and/or land, which is a common way to refer to these features, is a subjective definition which does not consider questions of scale and polynya functioning. In order to use climate models to investigate how Antarctic polynyas may change in the future, we need to both assess the impacts of different polynya definitions for gridded data and investigate how polynyas estimated from model output compare with those estimated from satellite images over the historical period. Objective and quantifiable methods to identify polynyas are necessary in order to assess their role in the climate and ecological system, compare observations with model output, and make inferences regarding future polynya change. Earth system models (ESMs) contributing to the Climate Model Intercomparison Project phase 6 (CMIP6) show a wide range of Antarctic sea ice states (e.g. Roach et al., 2020) and September polynya areas (Mohrmann et al., 2021). Open water polynyas show particularly large inter-model spread in size and frequency across all CMIP6 models, much of which may be due to differences in model hydrography and deep water convection, whereas differences in coastal polynyas is attributed at least in part to differences in horizontal resolutions and polynyas were identified across the models using the same thresholds regardless of grid resolution (Mohrmann et al., 2021). Biases in simulated Antarctic Sea ice will impact polynya identification as well – models that have very low mean sea ice states, for example, will consequently have a far smaller area over which it is possible for polynyas to form. ESMs struggle in particular to capture both small but significant positive observed trends in Antarctic Sea Ice, 1979-2015, and the more recent dramatic sea ice losses (Diamond et al., 2024; Roach et al., 2020). The recent, extreme losses and extended reconstructions of Antarctic sea ice suggest that there may be internal variability not captured by the relatively short observational record (e.g. Fogt et al., 2023; Hobbs et al., 2024; Holmes et al., 2024; and references therein).

Polynyas and polynya-like features often have scales and dimensions much smaller than those resolved by either satellite observations or global climate model data. Furthermore, sea ice concentrations (SICs) are calculated using different products and methodologies in observational data sets and climate model simulations. The long-term (since 1979) record of satellite SICs are retrieved from satellite microwave radiometers using sea ice algorithms. The retrieval algorithms differ in their sensitivity to sea ice temperature and emissivity, atmospheric conditions (including winds, cloud liquid water vapor content, humidity), surface roughness in open water areas and the sea ice state and presence of liquid water on the sea ice (e.g. melt ponds). Uncertainties in satellite-based SICs tend to be greatest in summer season, and regions of low sea ice concentrations (Ivanova et al., 2015). Climate model sea ice concentration data, on the other hand, are based on the physical evolution of simulated sea ice due to fluxes of energy and momentum. These differing definitions of the same field complicate comparisons of polynyas based on observational and model products. Passive microwave algorithms tend to underestimate SICs at low concentration levels and in thin ice areas (e.g. Meier, Windnagel and Stuart, 2021; Ivanova et al., 2015 and references therein), whereas climate model simulations calculate SICs to very small fractions and sea ice thicknesses (SITs) to very thin thicknesses, albeit with potential biases from forcing or structural model uncertainty. Additionally, satellite-derived SIT estimates remain spatially and temporally limited and have considerable uncertainty compared with SIC products (e.g. Kacimi & Kwok, 2022; Zygmuntowska et al., 2014 and references therein). Thus, SIT from satellite products has limited capacity for identifying thin sea ice which may be relevant for polynyas. In addition, climate model SICs and SITs are calculated at the model time-step (e.g. every hour) then averaged over a day for daily averages, whereas satellite microwave radiometer data represent an instantaneous snapshot of conditions (typically daily or bi-daily; Meier et al., 2014) specific to a particular time and location.

Previous studies have identified polynyas using various metrics and methods. In a study investigating the influence of various factors on the formation of polynyas in Eastern Antarctica, Massom et al (1998) found that a SIC threshold of 75% (where any grid cells below 75% SIC were identified as a polynya) worked well with the monthly 25kmX25km gridded satellite-based SICs to differentiate polynyas from the marginal ice zone. Arrigo & van Dijken (2003) used a satellite derived, downscaled (6.25kmX6.25km) passive microwave SIC product and utilized both concentration (10%) and time (>50% of winter days) thresholds to identify wintertime polynyas around the entire continent. The resulting polynya maps were further refined by whether neighbouring pixels merged later in the season to form larger “post polynyas”. Satellite-derived chlorophyll images (O’Reilly et al., 1998) have also been used to define “polynya regions” within which to further study phytoplankton dynamics, but satellite-based chlorophyll products can only identify polynyas in areas of both open water and clear skies. Tamura et al. (2006) proposed new algorithms for estimating sea ice thicknesses in thin sea ice areas and for differentiating thin sea ice from fast ice in the satellite radiometer data. The resulting maps of sea ice thicknesses in thin sea ice areas along with reanalysis data from both the European Centre for Medium-Range Weather Forecasts (ERA-40) and the National Centers for Environmental Prediction (NCEP2) were used to make maps of sea ice production and variability in Antarctic polynyas (Tamura et al., 2007; Tamura et al., 2015). This method of identifying thin sea ice areas was applied in work investigating the

influence of icescapes on Emperor penguin foraging habitat in East Antarctica (Labrousse et al., 2019). More recently, Mohrmann et al. (2021) identified polynyas using gridded SICs and SITs from 27 CMIP6 climate models, as well as the European Organisation for the Exploitation of Meteorological Satellites (EUMETSAT) Ocean and Sea Ice Satellite Application Facility (OSI SAF; Lavergne et al., 2019) satellite observations, to explore differences in open water and coastal polynya formation in climate models. Polynyas were identified by applying a <30% SIC threshold or <12 cm SIT threshold to all data on the respective native grids (which ranged from 25 km to 250 km nominal resolutions; Mohrmann et al., 2021). Duffy et al. (2024) applied a <50% SIC definition to daily satellite SIC data on a 25kmX25km grid to define polynya areas. These multiple working definitions of polynyas are not consistent, and to the best of our knowledge, no one has published work showing the implications of different polynya identification metrics applied to different data sources, at different spatial resolution, or over different temporal periods.

Our five primary goals in this work are to:

1. explore different methods of defining polynyas based on gridded time series data, and to define metrics that are reproducible, verifiable, and useful for assessing polynyas in present and future climate states,
2. use these optimal polynya metrics to identify coastal polynyas in satellite based sea ice products and an atmospheric-reanalysis forced ocean-sea ice (FOSI) simulation for comparison of the regional and seasonal identification of coastal polynyas in both satellite and simulated sea ice products,
3. assess the model marine biogeochemistry within the ice zone both within and outside of spring coastal polynyas to test if polynyas identify biological “hot spots” in the climate model
4. compare identification of coastal Antarctic polynyas over the historical time period between the FOSI configuration and a large ensemble of simulations of the fully coupled version of the model,
5. assess the internal variability in Antarctic coastal polynya areas and future trends.

We also seek to understand how choice of polynya metrics may influence results in terms of polynya area, frequency, trends and location. We intend for this exploration to give guidance on implications of various polynya metric choices for model and satellite-based data analysis. The role of low sea ice areas in Antarctic marine ecosystems is dynamic and diverse – polynyas affect availability of light and nutrients for phytoplankton, provide open water access and thus prey for marine predators such as penguins and seals, and the timing of low sea ice conditions influences the seasonal progression of phytoplankton blooms. In this paper, we investigate the impacts of metric choices on polynya identification, compare polynya areas estimated from simulated and observed data, assess if our polynya metrics identify biologically important marine regions, and apply these metrics to a large ensemble of historical and future climate scenarios. This analysis provides comprehensive and quantifiable information on polynya identification that can be used in future work to assess the role of changing polynyas on Antarctic marine ecosystem dynamics and the physical environment.

2 Data

2.1 Satellite observations

We consider two daily observational Climate Data Records (CDR) of gridded sea ice concentration data from satellite images: the CDR developed at the National Snow & Ice Data Center (NSIDC) for the National Oceanic and Atmospheric Administration (NOAA; Meier et al., 2014; Meier et al., 2021) and the European Organisation for the Exploitation of Meteorological Satellites (EUMETSAT) Ocean and Sea Ice Satellite Application Facility (OSISAF) CDR (Lavergne et al., 2019). The NOAA data are a merged product of the NASA Team and Bootstrap algorithms, with the higher SIC of the two products used as the CDR value when the two products differ (Meier et al., 2014). Both the NOAA CDR and OSISAF data are derived from the same satellite radiometer data but by using different sea ice retrieval algorithms. The largest differences in SICs resulting from different retrieval algorithms tend to be found in areas of relatively thin sea ice, where SIC tend to be underestimated across all algorithms (Ivanova et al., 2015; Kwok et al., 2007; Grenfell et al., 1992). We include both the NOAA and OSISAF products of sea ice concentrations in this study to explore differences in identified polynya areas from observationally-based gridded SIC products that may result due to different sea ice retrieval algorithms. Both the NOAA and OSISAF CDRs are used extensively in the research community. The NASA Team product typically has the lowest SICs in areas of thin ice of the different retrieval methods, and although the NOAA CDR uses Bootstrap SICs where NASA Team SICS are lower, we show one example of polynyas identified using the NASA Team product for comparison. The remainder of our analysis uses the NOAA and OSISAF CDR for our observationally-based gridded sea ice products.

We calculate polynya maps for the NOAA and OSISAF products on both the original (25 km x 25 km) Equal Area Scaleable Earth (EASE) grid as well as regridded onto a nominal 1° climate model grid, as described below. The reason to create maps on both grids is to better understand the impact of resolution on the identification of polynyas across different products (i.e. satellite observations and Earth System Models) that span large spatial scales. Additionally, given the differences in instantaneous satellite observations and model average conditions, we apply our polynya metrics to daily and monthly averaged data to better understand the impacts of temporal resolution on polynya identification.

2.2 Climate Model Output

This study uses output from the Community Earth System Model Version 2 (CESM2; Danabasoglu et al. 2020) for climate model data. We use model output from two different configurations of the CESM2: an ocean-ice hindcast forced by atmospheric reanalysis data, and a fully-coupled configuration forced by the Coupled Model Intercomparison Project Phase 6

(CMIP6) protocols for the historical (1850-2014) and future (2015-2100) high emissions scenario (SSP370; Eyring et al., 2016). Both CESM2 configurations are on the standard nominal 1° grid. The JRA-CESM hindcast simulation (Krumhardt et al., 2024) is a prognostic ice-ocean simulation with CESM2 that is forced by the Japanese Reanalysis product (JRA-CESM; Kobayashi et al., 2015; Tsujino et al., 2018) for atmospheric conditions. The fully coupled simulations (Danabasoglu et al., 2020) use a standard configuration that was a contribution to CMIP6 (Eyring et al., 2016) and have fully prognostic atmosphere, ocean, sea ice, and land components. We utilize the CESM2 50-member Large Ensemble (CESM2-LE, forced with the standard CMIP6 forcing (CESM2-LE; Rodgers et al., 2021).

For ocean biogeochemistry, both CESM2 configurations were run with the Marine Biogeochemical Library (MARBL) model (Long et al., 2021), which simulates planktonic marine ecosystem dynamics and coupled cycles of carbon, nitrogen, phosphorus, iron, silica, and oxygen. MARBL is highly configurable, allowing a flexible number of plankton functional types. In this study, the fully coupled simulation uses the planktonic MARBL ecosystem described in Long et al (2021), while JRA-CESM uses a slightly more complex ecosystem, described in Krumhardt et al. (2024). We focus on net primary productivity (NPP) here, which is the sum of net carbon fixation by all phytoplankton functional types. All configurations of CESM simulations compute light penetration based on a subgrid-scale sea ice thickness, important for capturing the non-linear photosynthetic function in ice-covered waters (Long et al., 2015).

The JRA-CESM hindcast simulation removes model-observational differences due to atmospheric forcing or internal variability. Thus, the simulated ice conditions and variability in the JRA-CESM are more directly comparable to the satellite products than the fully-coupled CESM and hence the bulk of our model-satellite polynya comparisons are based on this simulation. Antarctic SICs and sea ice extents (SIE; defined as the area covered by sea ice concentrations of 15% or higher) in the JRA-CESM compare well, spatially and temporally (Krumhardt et al., 2024), with the NSIDC Climate Data Record (Meier et al., 2021) and the NSIDC Sea Ice Index (Fetterer et al., 2017). The sea ice model (CICE) is a thermodynamic-dynamic model that resolves subgrid-scale ice thickness distribution in five sea ice thickness categories. CICE simulates thermodynamic (growth and melt rates of snow and ice from vertical conductive, radiative and turbulent heat fluxes) and dynamic (including advection and ridging) changes to sea ice concentrations and volume (Hunke et al., 2013). The sea ice component of the CESM2 used in all configurations shown here includes a “mushy” thermodynamic component that allows for a mixture of brine and solid ice which leads to increases in both frazil ice production and Antarctic Bottom Water formation in polynya-like coastal features when compared with the earlier model version, the CESM1 (DuVivier et al., 2021; Singh et al., 2020). Coastal frazil ice production is particularly important in Antarctic coastal polynyas (e.g. Nakata et al., 2021 and references therein). This paper presents a more in-depth view of polynyas in the CESM2.

3 Methods

3.1 Polynya algorithm

Our algorithm defines polynyas from a particular variable and threshold value. The two physical sea ice variables we focus on for polynya identification are SIC (observations and model) and SIT (model). Polynyas are identified as contiguous regions of grid cells that fall below a given threshold and are surrounded by land and/or ice-covered regions above the threshold (e.g. Appendix A). The first step in the algorithm identifies all grid cells that fall below the variable threshold and lie within the ice zone (i.e. not immediately bordering open ocean). In subsequent iterations, the algorithm checks neighbouring grid cells. If all grid cells bordering a region of ice below the threshold are bounded by higher threshold variables and/or land, then this region is identified as a polynya. If any neighbouring cells are bounded by open ocean, the grid cells are not considered a polynya even though they meet the threshold requirement. This iterative process is necessary in some regions and seasons when the northern ice edge may be complicated as polynyas open up and merge with open water (e.g. in the Ross Sea in austral spring and around the Western Antarctic Peninsula with a relatively complicated coastline). The polynya algorithm also numbers individual polynyas and calculates polynya areas based on the number of grid cells each individual polynya occupies. In this manner, we can calculate not only total polynya area by region, but also the number of individual polynyas and their sizes. This threshold-based algorithm is similar to the method employed by Mohrmann et al. (2023), but we identify polynyas for a range of threshold values for satellite-based SICs and model-based SICs and SITs. Our algorithm maps both open-water (surrounded by higher concentrations or thicknesses of sea ice) and coastal (at least one grid-cell neighbouring land) polynyas, but this work focuses primarily on coastal polynyas because of their important ecological functions and because open ocean polynyas are relatively uncommon in observations and in the model results.

We first explore the influence of polynya metrics on polynya identification in the satellite and JRA-CESM data by calculating integrated total polynya areas by different time periods (seasonal, annual, monthly) and region (Southern Hemisphere and smaller regions using the regional definitions of Parkinson & Cavalieri, 2012 and shown in Fig. 1f). We then choose one SIC and one SIT polynya threshold metric to apply to the 50-member CESM2-LE. These thresholds are based on the analysis of the integrated polynya areas from the satellite products and the JRA-CESM simulation compared with published estimates of Antarctic coastal polynya areas.

3.2 Impacts of metric thresholds, spatial and temporal resolutions on polynya identification

We apply a range of SIC (15%-85%) and SIT (10-85 cm) thresholds to identify polynyas in the two satellite products ("OBS") and the JRA-CESM on different spatial and temporal resolutions. Polynyas often have scales and dimensions much smaller than that resolved by standard gridded sea ice data, even the relatively fine resolution OBS data on a 25km^2 EASE grid. Thus, appropriate threshold values for identifying polynyas may depend on the size of the data grid cell. As a simplified example, a polynya defined by a 10% SIC threshold on a 6.25 km EASE grid (e.g. the sub-pixel grid used by Arrigo & VanDijken, 2003)

and surrounded by grid cells of 100% SIC would be classified as a polynya on 25/45 km EASE grids at 94/98% SIC thresholds (e.g. Appendix B). Polynya threshold choices are further complicated by climate model grids that tend to be in degrees latitude/longitude rather than equal-area grids. A given SIC threshold for the equal area grid is the equivalent of an area threshold (i.e. km^2 of open water within a grid cell), whereas on the equal-latitude/longitude grid a given SIC will correspond to different total open water areas within a grid cell depending on latitude (since the grid cell surface area is latitude-dependent, and thus a percentage of the total grid cell area will represent a different area depending on latitude; see Appendix B). Given these considerations and the scientific question at hand, the threshold used may need to depend on grid size and may be specific to region, season, and variable. We explore the impacts of grid size on polynya areas by making polynya maps from different grid sizes in the satellite data – the original 25 km EASE grid and regridded to the standard nominal 1° CESM grid. We compare polynya metrics between satellite and climate model output by focusing on the regridded satellite data.

Polynya-like features can change rapidly in time, particularly for wintertime Antarctic coastal polynyas when surface air temperatures are extremely cold and extensive (albeit thin) sea ice can form rapidly at open water surfaces. Polynyas identified from daily data, for example, may not appear on monthly time scales (particularly in the model, which can simulate high concentrations of very thin sea ice). We investigate the effects of temporal resolution on polynya identification by comparing polynyas estimated from daily and monthly data in both the satellite product and the model output.

3.3 Impacts of differing methodologies for calculating sea ice concentrations in the model and satellite images

Comparing polynya estimates in models and satellite observations is not a trivial matter. Passive microwave retrieval algorithms struggle to detect sea ice when concentrations fall below ~10%. As a result, the National Snow & Ice Data Center (NSIDC) Climate Data Record (CDR) implements a 10% minimum threshold on the CDR data product (Meier, Windnagel and Stuart, 2021). Satellite-based SICs are underrepresented in areas of thin sea ice across all retrieval algorithms, particularly where sea ice thicknesses are below 25 cm (Ivanova et al., 2015). Sea ice between 5 and 20 cm thick will result in systematically underestimated SICs (Ivanova et al., 2015). In contrast, climate model simulations calculate SICs to very small fractions independent of mean SIT. This complicates how a polynya is identified in each dataset. For example, winter-time polynyas can be regions of extremely high sea ice production where sea ice forms nearly as fast as winds expose water to the overlying atmosphere. In these conditions, one might expect polynya metrics based on SIT would be more appropriate than SIC in model output as the extreme cold wintertime air temperatures can lead to nearly immediate sea ice formation and thus high SICs even if SITs are very thin. Conversely, SICs are underestimated in satellite products when the ice is very thin, so a satellite observation in these conditions should show lower SIC (note that observations of SIT are very limited). This is a clear example where SICs may be better suited for defining wintertime polynyas from satellite images whereas SITs might be a better metric from climate model output.

Given the challenges of passive microwave measurements and retrieval algorithms to estimate sea ice concentrations in low concentration and thickness conditions, as detailed above, we explore the influence of different definitions for SIC in satellite-based observations and model output by degrading the JRA-CESM hindcast sea ice concentrations such that the modified SICs are more closely aligned with SICs as they would be remotely sensed. Model SICs are degraded by setting daily SIC in grid cells with less than 10% SIC or less than 5 cm daily SIT to 0% SIC, closer to the values that a satellite would observe in these conditions. Daily SICs within grid cells that have SITs of 5-20 cm thick are set to half of the original model SIC output, which corresponds to the underestimation of ice concentration over thin ice by satellites (Appendix C). Although using daily averaged data is not the same as the instantaneous satellite-snapshot data, it is the highest frequency model output of sea ice data available. We compare the degraded model SIC to the original output to gain insight into how differences in SIC methodologies may impact polynya identification in both observed and model data products.

3.4 Influence of metrics and resolutions on polynya identification

One of our primary goals in this work is to better understand how different metric choices on a variety of gridded data products will influence polynya identification, and how to best compare polynyas identified in both observational and simulated data. We explore both the influence of resolutions (temporal and spatial grid size) and metric thresholds. We identify polynyas over a range of SIC thresholds (15%-85%) throughout the year in the satellite based observations on the original EASE grid, regridded to the nominal 1° model grid, and on both daily and monthly-averaged data. Similarly, we apply the same range of SIC thresholds as well as a range of SIT thresholds (10-85 cm) to the daily and monthly JRA-CESM. We analyze these results by month and on regional and hemispheric scales to elucidate how the influence of polynya identification metric choice may differ by time of year and region.

Based on the analysis of the NOAA and OSISAF CDRs and JRA-CESM, we pick two polynya identification metrics (85% SIC and 0.4 cm SIT thresholds on monthly averaged sea ice data) to apply to the 50-member CESM2 over the historical (1850-2014) and future scenario (2015-2100) time periods. These polynya time series serve as the basis for our exploration of changes in both polynyas and NPP within polynyas in the future climate.

3.5 NPP and polynyas

Polynyas play important roles in physical and biological processes, and optimal metrics for defining polynyas may differ depending on analytical goals. Here we explore what constitutes an optimal model-derived polynya metric based on their ecosystem-relevance, specifically their relation to NPP. During the austral spring (September-October-November), sea ice is melting and directly impacting NPP through light availability. During this season the optimal choice of metric (SIT or SIC) to define polynyas is not clear, and as such we pick one metric based on SIC and another on SIT to identify polynyas and investigate if these springtime polynya areas have increased productivity in the JRA-CESM model simulations by calculating NPP both within the polynya areas and within the sea ice zone (SIZ) as a whole. The SIZ is defined as the region south of the mean wintertime (June-July-August) northern pack ice (SIC $\geq$85%) boundary. Thus, regions within the ice pack and near the

coast that may have lower sea ice concentrations (e.g. polynyas) lie within the SIZ. The goal is to help inform choices in future studies particularly when using model output that may not include marine biology components or that do not allow for trophic transfers to higher trophic levels as is critical for high latitude, light-limited systems.

3.6 Polynyas and NPP in a changing climate

In this section we explore how both polynyas and NPP change from the historical time period into the future under the SSP3-7.0 emissions scenario. We compare results from the CESM2-LE during the historical period with results from the JRA-CESM and the CDR satellite records for context. We calculate integrated hemispheric NPP both within the SIZ and within springtime polynyas in the CESM2-LE, comparing both timeseries throughout the historical and future scenarios, and the climate mean annual cycle of NPP at the beginning (2001-2020) and end (2081-2100) of the 21st Century. We leave analysis of how future changes in NPP may be related to changes in trophic transfer and phytoplankton function types to future work.

4 Results

4.1 Large-scale sea ice properties

The JRA-CESM and the CESM2-LE generally capture observed Southern Hemisphere (SH) sea ice area means as well as temporal and spatial variability quite well compared to CMIP6 models (e.g. Roach et al., 2020). Both versions of the model used for this study underestimate total SH sea ice areas (SIA) from July through October by ~10-14% (~1.4-2.6 x 10^6 km^2) compared with both the NOAA and OSISAF products (Fig. 1e; NOAA and OSISAF sea ice areas are only slightly different – Supplemental Figure 2 – so only the NOAA CDR is shown here). Regionally, both the ocean-ice and fully coupled model simulations tend to underestimate Antarctic sea ice in the Weddell Sea for all months of the year and in the Indian sector in the winter through spring months (Fig. 1 and Supplemental Fig. 1). The largest differences between the JRA-CESM and fully coupled CESM2-LE datasets are found in the Weddell sea and Indian sectors. During the austral summer in the Weddell Sea, the CESM2-LE has substantially more sea ice than the JRA-CESM although still less than the satellite products. From winter through spring, the CESM2-LE underestimates sea ice in the Indian sector compared with both OBS, however the JRA-CESM simulates more sea ice in this region than the CESM2-LE particularly during the winter. The CESM2 simulations represent a reasonable selection of climate model for identifying Antarctic polynyas because both JRA-CESM and CESM2-LE fully coupled configurations capture the mean climatology of Antarctic sea ice, particularly compared with CMIP6 models (Roach et al., 2020) and simulate coastal polynya-like features of high sea ice production (Singh et al., 2020; DuVivier et al. 2021).

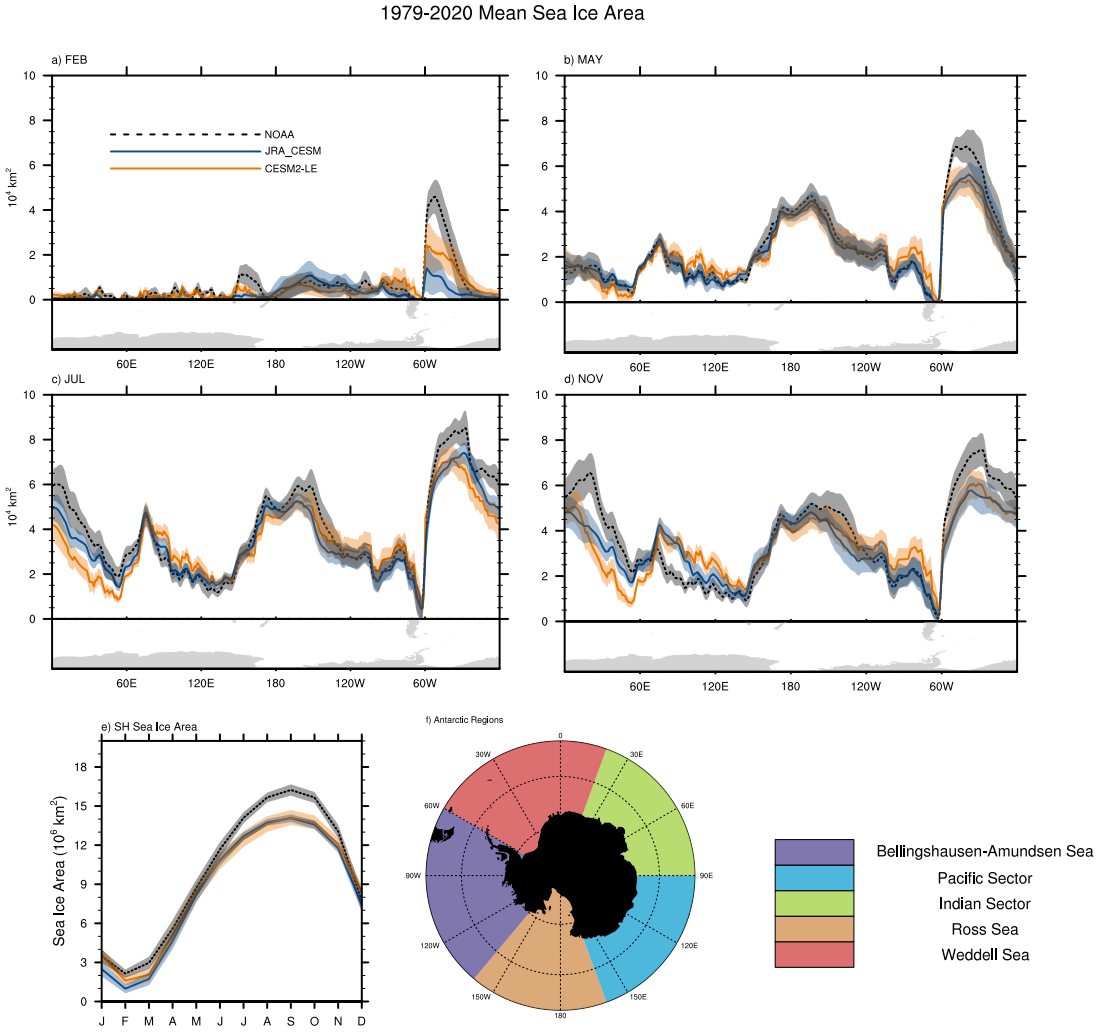

Figure 1. 1979-2020 Monthly mean total sea ice area as a function of longitude for a) February, b) May, c) July, d) November; e) monthly Southern Hemisphere (SH) sea ice area climatology for the NOAA CDR (black), JRA-CESM (blue) and CESM2-LE (orange) data; and f) Antarctic regions map. Thick dashed (NOAA) and solid (JRA-CESM, CESM2-LE) lines indicate the mean (or ensemble mean for the CESM2-LE), shaded polygons indicate the mean ±1 standard deviation. Sea ice areas as a function of longitude have been smoothed by a 3-point running average.

4.2 Polynyas in the satellite data

Maps of open water and coastal polynyas on July 15, 2003, calculated using our algorithm and a SIC threshold of 85% for observational datasets are shown in Fig. 2 (a-e). Note that this date is not special, but a representative day shown to illustrate differences in polynya identification metrics across products. We picked a random winter day as relatively few polynyas are identified in January-April in all data products (Supplemental Figs. 2-3), polynya area variabilities increase substantially for

all metrics in November-December, and the broad similarities and differences between polynyas identified in different data products on this winter day are typical.

polynyas JUL 15 2003

NOAA

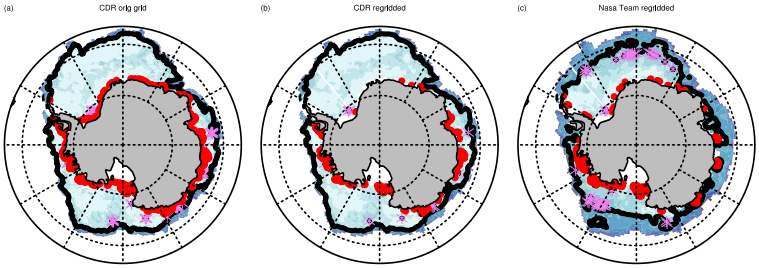

OSISAF

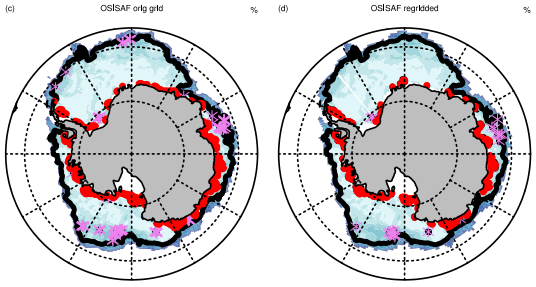

SIC (%)

5 20 50 80 95

JRA_CESM (85% and 0.4m thresholds)

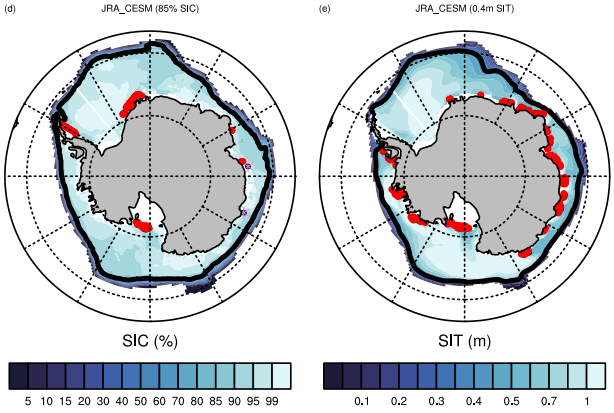

threshold ● Coastal polynyas ✳ Open Water polynyas

Figure 2. Polynya maps for July 16, 2003 using SIC 85% threshold and the NOAA and OSISAF CDR data on the original Equal Area Scaleable Earth (EASE) grid (a, d), the OBS regridded to the CESM grid (b, e), the NASA Team SIC product regridded to the CESM grid (c), and the JRA-CESM (f) and the JRA-CESM using a 0.4m SIT threshold (g). Open water and coastal polynyas are indicated by the pink stars and red dots. The 85% SIC and 0.4m contours are indicated by the thick black contours over the colour-contoured SIC or SIT values. Sea ice concentrations below 15% are masked out.

The sea ice edge (defined as the 15% SIC contour) is nearly identical for all satellite products – NOAA and OSISAF CDRs on the original grid, regridded to the nominal 1° climate model grid, and the NASA Team satellite product - even though the edge of the pack ice (defined as 85% or higher SIC) is much further away from the sea ice edge in the NASA Team product (Fig. 2a-e). More open water polynyas are identified in the OSISAF product than the NOAA. Differences in coastal polynyas identified in the two satellite products are more mixed, with more coastal polynyas identified on the east side of the Antarctic peninsula in the OSISAF CDR than in the NOAA CDR, regridded or not, yet more coastal polynyas in the Weddell Sea in the NOAA product on the EASE grid than in the OSISAF. Regridding has a greater impact on polynya areas in the NOAA product than on the OSISAF product (Fig. 2 a,b,d,e and Fig 3 a, b). In general, NASA Team SICs are often lower than those of both OBS and result in a larger number of polynyas identified for a given threshold SIC when the products are on identical grids. The regridded NASA Team data also show more open water polynyas using the 85% threshold than either the regridded NOAA or OSISAF CDR data (Fig. 2b-c, e). This is likely because the NASA Team algorithm tends to underestimate SICs, particularly during the melt season (Comiso et al., 1997; Meier, 2005). We show both open water and coastal polynyas identified in our example day, however we focus on coastal polynyas for the remainder of this study.

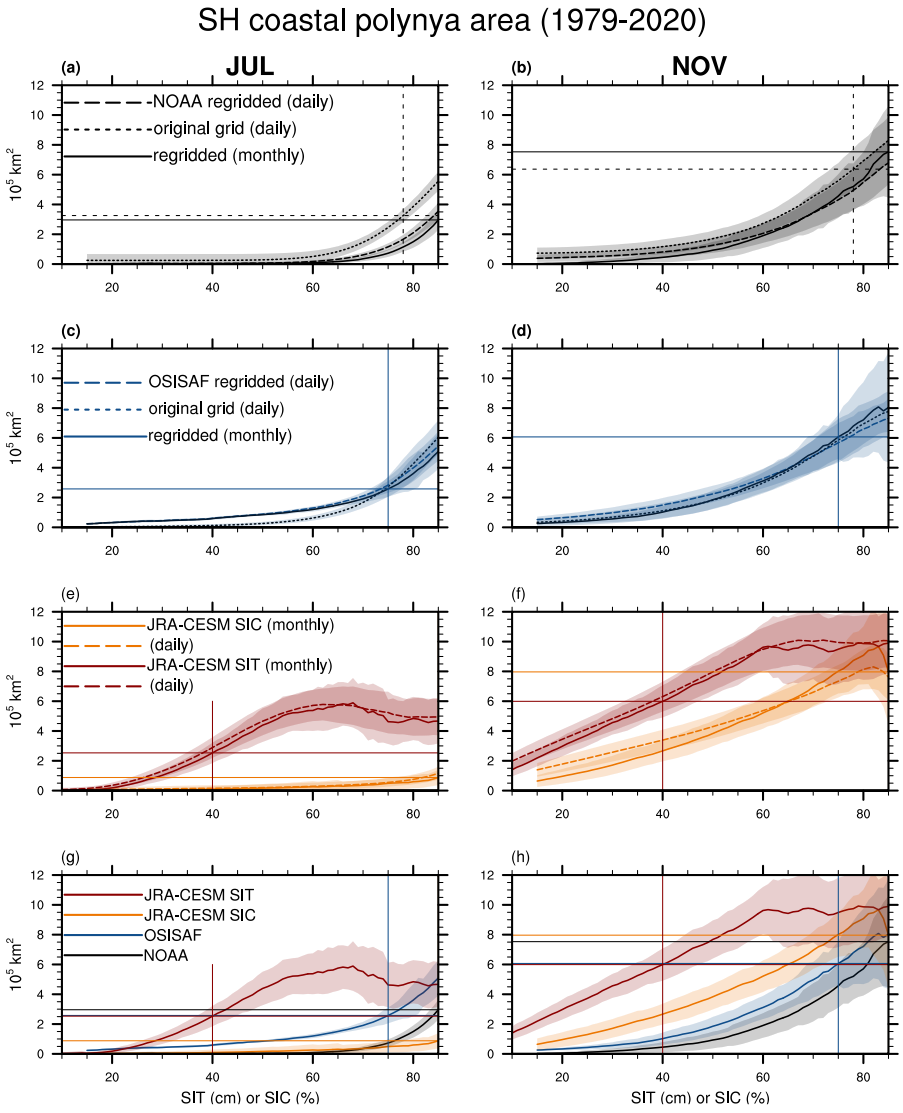

Figure 3. Total SH coastal polynya area as a function of SIC threshold for July (left column) and November (right column) for NOAA CDR (top; a-b), OSISAF CDR (second row; c-d), JRA-CESM (third row, e-f) and both OBS and JRA-CESM monthly (e-f). Results showing those using monthly data from both satellite products and the JRA-CESM are shown together in panels g-h for reference. Results using daily/monthly data are shown by dashed/solid lines, and results from the satellite products on the original EASE grid are shown by dotted lines. Colours correspond to NOAA (black) and OSISAF (blue) data; and the JRA-CESM using SIC (orange) and SIT (brown). Climatological mean (1979-2020) values are shown in the thick lines; ±1 standard deviations shown by the lighter shading. Horizontal lines indicate mean polynya areas at SIC thresholds of 78% (NOAA daily, black), 85% (NOAA monthly, black), 75% (OSISAF monthly, blue), 85% (JRA_CESM SIC monthly, orange) and 0.4m SIT (JRA-CESM SIT monthly, dark maroon). Vertical lines indicate 0.4m SIT and 75% SIC for reference.

4.2.1 Integrated Southern Hemisphere polynya areas, numbers and sizes in the satellite data

When moving beyond an example day and looking across all years, the primary differences in integrated total SH area of coastal polynyas in the NOAA CDR as identified by SIC threshold values arise from grid resolution during the late fall through early spring (May-October; Fig. 3 a-b and Supplemental Fig. S3). Integrated southern hemisphere (SH) coastal polynya areas are larger for a given threshold in the NOAA product on the original higher-resolution EASE grid than when regridded to the 1° CESM grid from April through October. Polynya areas in the NOAA product are nearly the same using both the regridded daily and monthly averaged data. On the other hand, regridding either spatially or temporally has little effect on integrated SH polynya areas identified in the OSISAF CDR (Figure 2 b-c and Supplemental Figure S4). Variability in SH polynya areas tends to be larger during the ice retreat season November-January) in both CDRs (Fig. 3b, d and Supplemental Figs. 3-4). Throughout most of the year, differences due to temporal resolution are much quite small at a given threshold. More grid cells are identified as polynyas in the NOAA CDR, and the total SH polynya area is larger on the original, smaller resolution EASE grid than on the regridded data for a given threshold value. A given SIC threshold in the monthly regridded data identifies a larger SH polynya area in the OSISAF CDR than in the NOAA CDR.

To better compare relationships between polynya area means, variability, trends, seasonalities and regionalities across the OBS and the climate model, we use polynya metrics and thresholds that result in total 1979-2020 climatological SH polynya areas similar to those estimated from observations in other studies (e.g. Arrigo & Van Dijken, 2003; Tamura et al., 2008; Nihashi & Ohshima, 2015). The metrics and thresholds we use for the satellite products are SIC threshold values of 78% and 85% for the EASE daily and regridded, monthly NOAA CDR data, and 75% for the OSISAF CDR. Although in general the integrated SH polynya areas are very similar between these metric choices in these data products, there are some small differences in areas, numbers of polynyas, and variabilities (Table 1, Figure 4 and Supplemental Figures 3-4, Supplemental Figure 6). Notably, a larger number of distinct polynyas are consistently identified in the OSISAF data than in the NOAA data (regridded to the 1° grid and monthly averaged), and thus even though the SH polynya areas are quite similar, the average polynya size in the OSISAF is smaller than in the NOAA product (Table 1). The number of polynyas identified in the OBS on the EASE grid is roughly twice as large as the number identified on the 1° model grid (Table 1), underscoring a possible complication when comparing polynyas estimated from different grid sizes (e.g. Appendix B). Additionally, variability in November SH polynya areas is more than double in the NOAA CDR than in the OSISAF CDR. Trends in wintertime (July) SH polynya areas are significant and negative across the satellite products, however the November trends are not significant in the NOAA regridded monthly data, whereas they are negative and significant in the OSISAF data and the NOAA data on the original EASE grid.

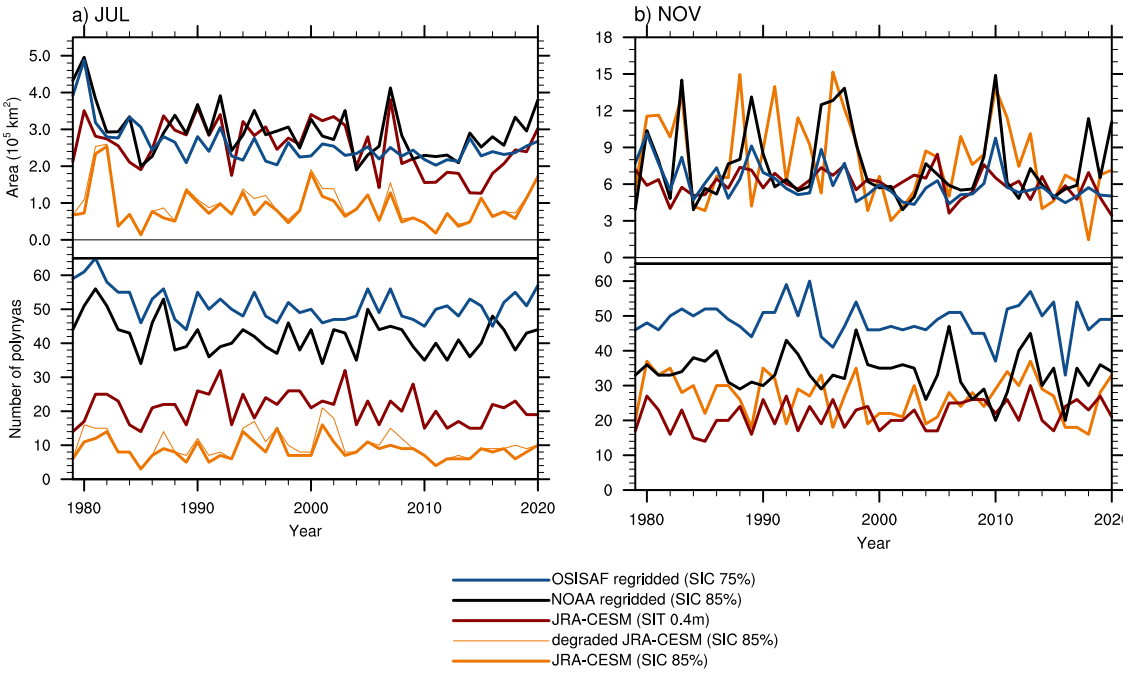

Figure 4. Southern Hemisphere (SH) 1979-2020 July (a) and November (b) mean coastal polynya area (top panels) and number of individual polynyas (bottom panels). Polynya timeseries are for monthly NOAA (SIC 85%; black) and OSISAF (SIC 75%; blue) CDR data regridded onto the CESM grid, JRA-CESM model simulation using monthly SIC (85%; orange) and SIT (0.4m; brown), and the JRA-CESM model SIC degraded to more closely mimic satellite SICs (85%; orange thin line).

1979-2020 SH coastal polynya mean area, mean number, and trends

	Data, threshold	July	November	ANN
polynya area (10^3 km^2)	NOAA 85% SIC	296 (66)	753 (307)	275 (31)
	NOAA EASE grid 78% SIC	326 (44)	637 (138)	308 (28)
	OSISAF 75% SIC	258 (53)	607 (147)	251 (35)
	OSISAF EASE grid 75% SIC	273 (68)	586 (141)	271 (35)
	JRA-CESM 85% SIC	88 (51)	797 (349)	201 (35)
	JRA-CESM 0.4m SIT	253 (68)	599 (108)	297 (43)
# polynyas	NOAA 85% SIC	42 (5.3)	34 (5.8)	29 (2.6)
	NOAA EASE grid 78% SIC	83 (15.4)	64 (14)	57 (12.4)
	OSISAF 75% SIC	51 (4.8)	49 (5.1)	38 (2.1)
	OSISAF EASE grid 75% SIC	55 (7.1)	44 (4.7)	38 (3.2)
	JRA-CESM 85% SIC	8.5 (2.9)	27 (6)	9 (1)
	JRA-CESM 0.4m SIT	21 (4.6)	22 (4)	15 (1.3)

Mean polynya size (10^3 km^2)	NOAA 85% SIC	7.0	22.3	9.6
	NOAA EASE grid 78% SIC	3.9	10.0	5.4
	OSISAF 75% SIC	5.1	12.4	6.6
	OSISAF EASE grid 75% SIC	5.0	13.3	7.1
	JRA-CESM 85% SIC	10.4	30.0	21.4
	JRA-CESM 0.4m SIT	12.0	27.6	19.9
Polynya area trends (10^3 km^2/decade)	NOAA 85% SIC	**-15.1**	3.8	-6.6
	NOAA EASE grid 78% SIC	**-13.3**	**-35.6**	-5.9
	OSISAF 75% SIC	**-15.5**	**-46.5**	**-13.7**
	OSISAF EASE grid 75% SIC	**-28.0**	**-46.3**	**-13.7**
	JRA-CESM 85% SIC	-2.4	-68.2	**-9.5**
	JRA-CESM 0.4m SIT	**-21.4**	-15.4	**-10**
# polynya trend (#/decade)	NOAA 85% SIC	-0.1	0.1	**-0.9**
	NOAA EASE grid 78% SIC	**-7.0**	**-6.4**	**-4.5**
	OSISAF 75% SIC	-1.1	0.1	0
	OSISAF EASE grid 75% SIC	**-1.1**	**-2.0**	**-3.0**
	JRA-CESM 85% SIC	0	-0.1	0
	JRA-CESM 0.4m SIT	0	**0.1**	**0.5**

Table 1. Climatological Southern Hemisphere (SH) polynya area mean (and standard deviation), number of polynyas mean (and standard deviation), average polynya size and Theil-Sen non-parametric linear trend in total polynya area and number of polynyas for polynyas identified on the CESM nominal 1° grid and monthly data except where otherwise specified. Bold text indicates trends that are at 95% or higher significance based on the Mann-Kendall non-parametric trend significance (Mann 1945; Kendall 1975; Gilbert 1987).

We also calculated correlations for SH polynya area timeseries, by month, for the satellite products and JRA-CESM to further evaluate similarities and differences (Figure 5). Although the correlations for polynyas identified from both the NOAA and OSISAF are significant across the three grids (EASE, regridded daily, and monthly averages of regridded daily), the magnitudes show quite a large range, with the lowest correlations seen in the NOAA timeseries between the two regridded data (daily vs monthly). Correlations are generally highest during the late winter and spring months (June-November), and generally higher between the OSISAF timeseries than the NOAA timeseries. Correlations are lower between the CDRs (c) than within the CDRs (a) for most months and grids (spatial, temporal) and SH polynya areas identified in the NOAA and OSISAF monthly data on the 1° model grid are not significantly correlated for either April or October. This is somewhat astonishing that the same passive microwave measurements but different retrieval algorithms can lead to uncorrelated timeseries of SH polynya areas once the data have been regridded and averaged by month. Additionally, correlation coefficients between the OBS, although significant, are less than 0.75 for all grids from April to October, suggesting considerable

variability in the time series due to the nuances of the retrieval algorithms. Curiously, integrated SH polynya areas estimated using the NOAA CDR on the original grid have significant negative trends in November, however not in the regridded product (Figure 5 and Table 1), whereas November SH polynya area trends are significant and negative across all three OSISAF polynya areas (EASE, daily regridded, monthly regridded). Indeed, there are significant negative trends in the OSISAF SH polynya area timeseries for all months except December; in the NOAA-derived polynya time series, however, the only significant trends – also negative – occur in only 4 months – February, March, July and November.

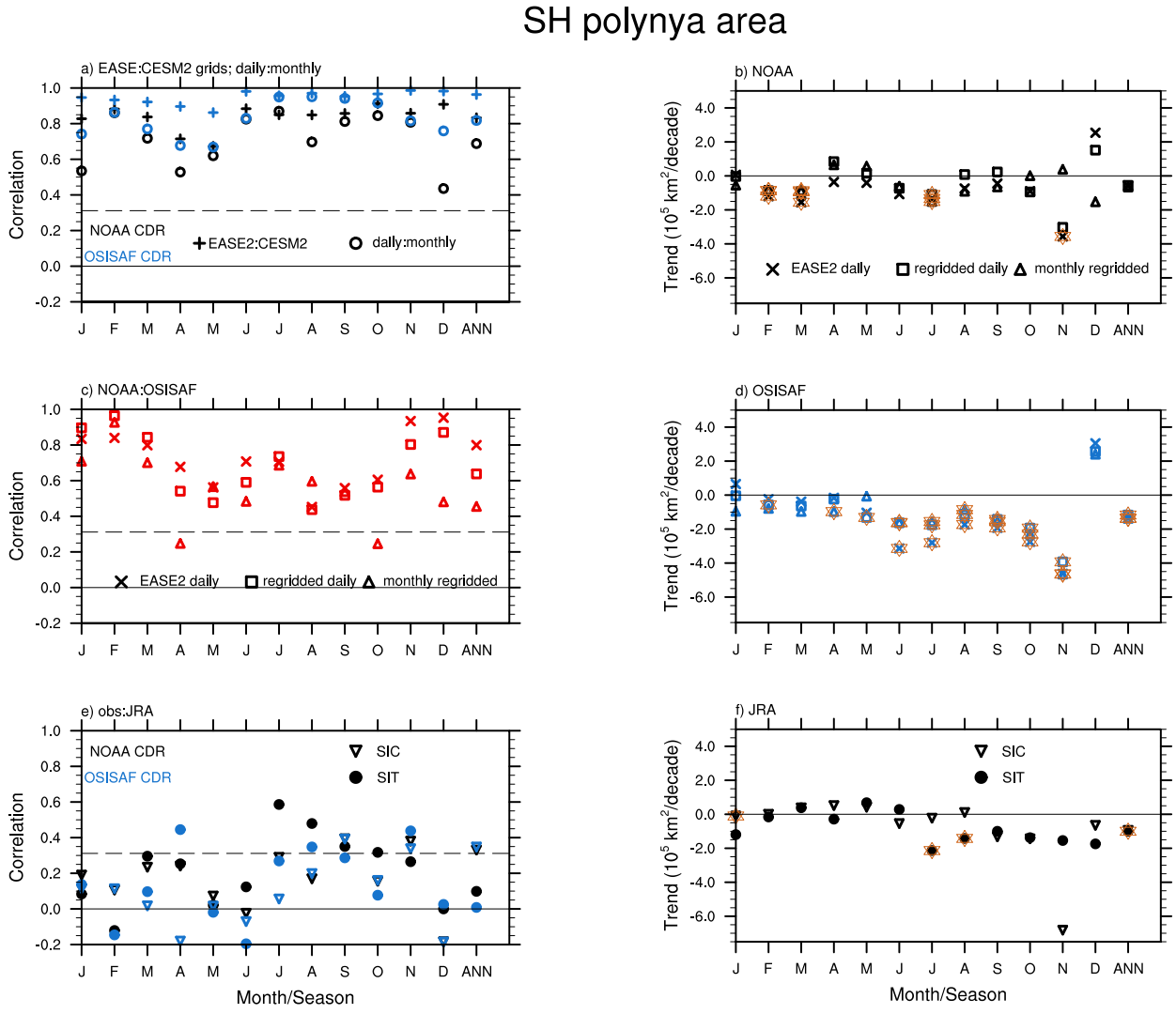

Figure 5. Correlation coefficients (left column) and trends (right column) for integrated SH polynya area for each month of the year and the annual average. Correlations are calculated between different grids for the NOAA and OSISAF data (a), between the NOAA

and OSISAF data (b), and between the NOAA, OSISAF and JRA-CESM (all monthly and on the nominal 1° grid; (c). Plus (+) symbols in (a) indicate correlation coefficients between polynyas identified using the CDR on the EASE grid and regridded to the model grid, and open circles mark correlation coefficients between regridded monthly and daily data (NOAA correlations shown in black, OSISAF shown in blue). Middle correlation panel (c) shows the correlations between the NOAA and OSISAF CDR for the daily data on the EASE grid (X's), the daily data regridded to the 1° model grid (open squares), and the monthly CDR data on the model grid (open triangles). Correlations with SH polynya area timeseries from the JRA-CESM are shown for NOAA (black) and OSISAF (blue) for polynyas calculated using SIC 85% concentration threshold (upside down open triangles) and the 0.4 m thickness threshold (closed circles). Trends are shown for NOAA (b) and OSISAF (d) for daily data on the EASE grid (X's), regridded daily data (open sqares), and regridded monthly data (open triangles). Trends for SH polynya areas from the JRA-CESM (f) are shown for polynyas identified using the monthly SIC (85%; open triangles) and SIT (0.4m; closed circles). Dashed horizontal lines in a, c, e indicate the 95% significance level based on the Mann-Kendall non-parametric trends significance (Mann 1945; Kendall 1975; and Gilbert 1987). Significant trends (b,d,f) are indicated by the gold stars.

4.2.2 Regional polynyas in the satellite data

Winter (July) and spring (November) polynya areas as a function of longitude show both similarities as well as differences resulting from choice of CDR (NOAA vs OSISAF), temporal and spatial grids (Figure 6). Higher polynya areas are identified, for example, by the NOAA data in the Ross Sea region in November, and in the OSISAF product near the Antarctic peninsula in November and particularly in July. In general, polynya areas identified using the regridded daily product are higher in both CDRs than those identified using the data on the EASE grid or the monthly regridded data – the exception to this is the Ross Sea in November, when higher polynya areas are identified in both products using the monthly, regridded data. November sea ice is both highly variable and rapidly retreating (Fig. 1e), and the Ross Sea polynya often merges with the open ocean during November (not shown) – polynya areas identified using daily data can become "open water" overnight and the daily polynya area will suddenly drop, whereas the monthly averages may capture, on average, a higher polynya area due to smoother seasonal transitions of the ice pack resulting from monthly averaging.

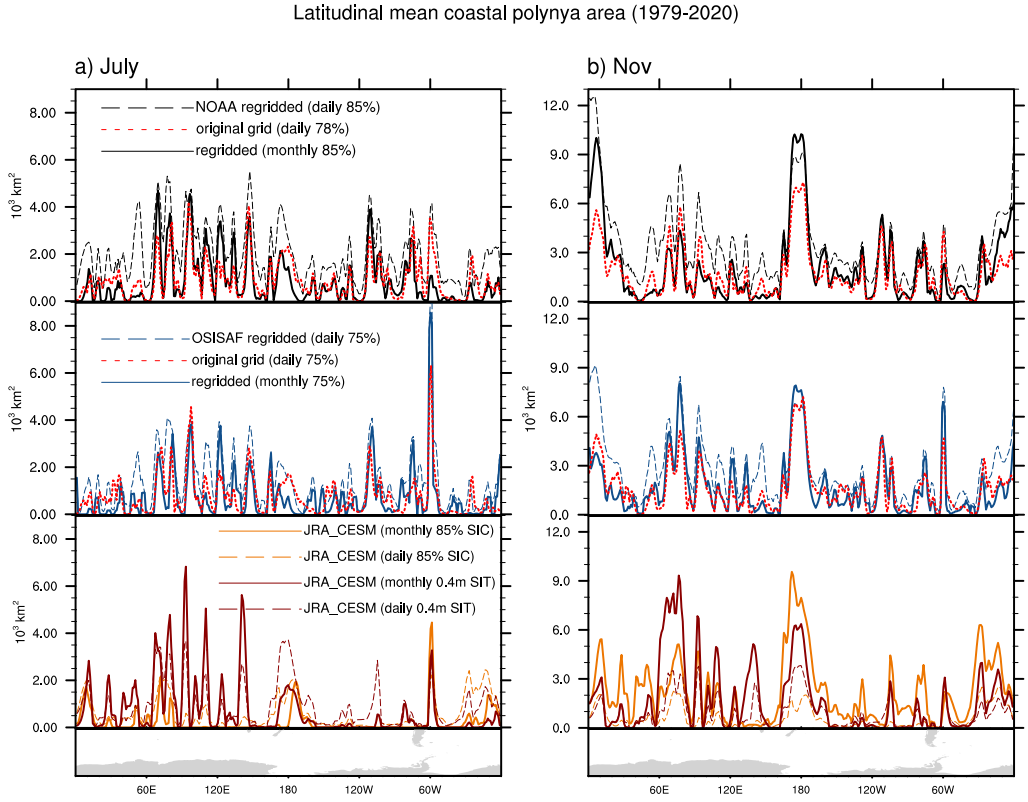

Figure 6. Monthly mean coastal polynya area as a function of longitude for July (a) and b) November (b) for the NOAA CDR (top), OSISAF CDR (middle) and JRA-CESM (bottom). Polynya area as a function of longitude is shown as a 3° (longitudinal) running average. Top and middle panels show polynya areas for the three different grids and metrics - daily NOAA (78% SIC) and OSISAF (75% SIC) on the original grid (red dotted lines), CDR daily data regridded onto the CESM grid (NOAA 85% SIC black and OSISAF 75% blue) dashed lines, and regridded and monthly averaged (NOAA 85% SIC, black and OSISAF 75%, blue) solid lines. Bottom panels in a) and b) show polynya areas based on JRA-CESM model simulation using different polynya thresholds: monthly (solid lines) and daily (dashed lines) SIC at 85% threshold (orange) and monthly SIT at 0.4m (brown) thresholds.

Climatological, coastal polynya areas as a function of longitude from the OBS data products on different grids are significantly correlated for all months across geographic (EASE, regridded) and temporal resolutions (daily and monthly), although regridding from the original EASE grid onto the 1° model grid lowers the regional correlations for the both products and particularly for the OSISAF, April-October. (Figure 7). Furthermore, longitudinal correlations between the monthly regridded CDR (NOAA:OSISAF) products lie between 0.4 and 0.6 for fall through early spring (April through October), and correlations between the OBS are generally lower than they are within an observational product, highlighting that both regridding (geographical and temporal) and different retrieval algorithms can result in different regional polynya identifications. Correlations of regional timeseries of polynya areas give more insight into differences in polynyas identified in the two CDRs:

correlations are highest between the OBS for the Bellingshausen-Amundsen Sea where the only correlation that is not significant is found in April between the two monthly, regridded products (Figure 8 and Supplemental Figure 7). All other sectors have multiple months and/or grids when regional timeseries from the two OBS are not significantly correlated – in fact 20% of the time the regional polynya timeseries from the regridded monthly data are not significantly correlated (Figure 8). Temporal correlations between the two OBS in regional polynya timeseries are particularly lower in the Weddell and Pacific sectors in the spring-winter (Wedell; April-August) and winter (Pacific; July-August), respectively.

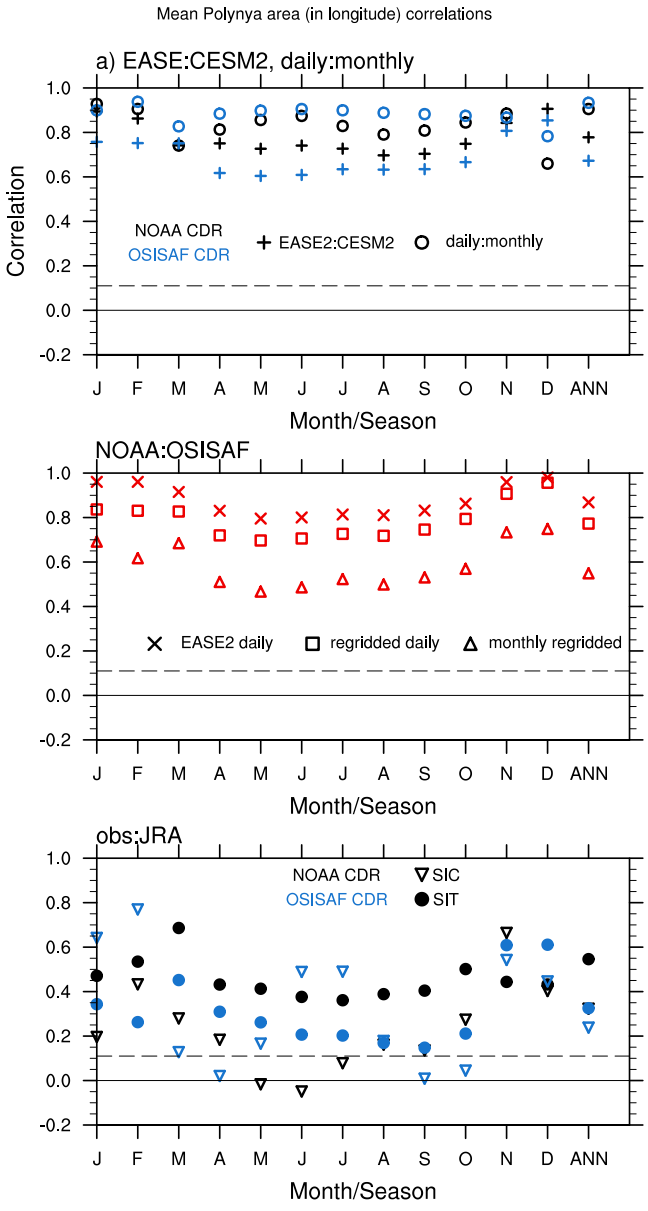

Figure 7. Correlation coefficients for polynya areas as a function of longitude for each month of the year and the annual average. Correlations are calculated between different grids for the NOAA and OSISAF data (a), between the NOAA and OSISAF data (b), and between the NOAA, OSISAF and JRA-CESM (all monthly and on the nominal 1° grid; (c). Plus (+) symbols in (a) indicate correlation coefficients between polynyas identified using the OBS on the EASE grid and regridded to the model grid, and open circles mark correlation coefficients between regridded monthly and daily data (NOAA, black; OSISAF, blue). Middle correlation panel (c) shows the correlations between the NOAA and OSISAF for the daily data on the EASE grid (X's), the daily data regridded to the 1° model grid (open squares), and the monthly OBS data on the model grid (open triangles). Correlations with SH polynya area timeseries from the JRA-CESM are shown for NOAA (black) and OSISAF (blue) for polynyas calculated using SIC 85% concentration threshold (upside down open triangles) and the 0.4 m thickness threshold (closed circles). Dashed horizontal lines indicates the 95% significance level.

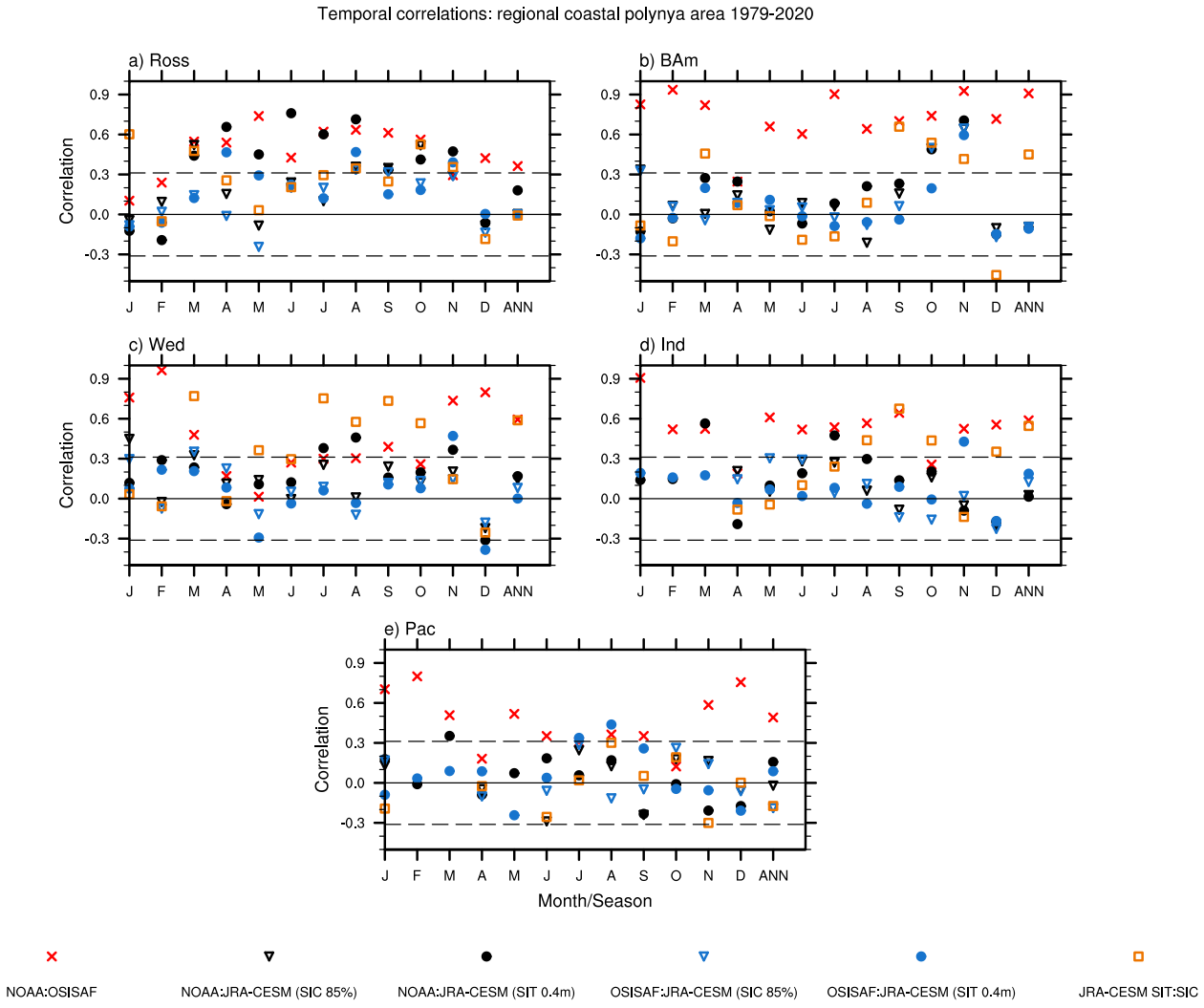

Figure 8.Temporal correlation coefficients for regional polynya area timeseries for each month of the year and the annual average. Correlations are calculated between monthly timeseries on the model grid: NOAA:OSISAF (red Xs), OBS:JRA-CESM are shown in black (NOAA:JRA-CESM) and blue (OSISAF:JRA-CESM) for SIT (open triangles) and SIC (solid circles) polynya identification metrics; and JRA-CESM SIT:SIC (orange squares). Dashed horizontal lines indicates the 95% significance level.

Regional trends in polynya areas for July, November and Annual averages show significant negative trends in both OBS regardless of temporal and geographic grids only for July and annually for the Bellingshausen-Amundsen sea (Table 2). Polynyas identified in the Ross Sea region in July and both the Ross and Weddell Sea regions in November show significant declines in area 1979-2020 for both OBS, however only in the polynyas identified on the original EASE grid for the NOAA CDR. If all months of the year are considered, trends are significant and consistent in both OBS from April through

November/September for the Ross/Bellinghausen-Amundsen Sea (Supplemental Figures 7-11). Strikingly, trends are significant and of opposite signs in August-September in the Pacific sector for polynyas identified in the OSISAF (negative) and NOAA (positive) products even while the Pacific sector time series are significantly correlated (Figure 8 and Supplemental Figures 7-11). This suggests that different retrieval algorithms are estimating different variations in sea ice concentrations within the icepack that lead to differences in region polynya areas.

Coastal polynya area (10^3 km^2) and trends (10^3 km^2/decade)

Region	Data, threshold	July		November		Annual	
		Area (std)	Trend	Area (std)	Trend	Area (std)	Trend
Ross	NOAA 85% SIC	41 (17)	-3.1	232 (88)	-10.4	58 (21)	-3.3
	NOAA EASE grid 78% SIC	60 (12)	**-3.7**	168 (47)	**-17.0**	72 (15)	**-3.4**
	OSISAF 75% SIC	30 (8)	**-2.6**	160 (65)	**-24.0**	50 (23)	-3.2
	OSISAF EASE grid 75% SIC	44 (14)	**-5.7**	158 (50)	**-20.9**	61 (16)	**-6.3**
	JRA-CESM 85% SIC	17 (11)	-1.5	234 (144)	9.7	42 (14)	0.3
	JRA-CESM 0.4m SIT	30 (19)	-2.5	128 (43)	-3.5	75 (31)	-2.8
Bellingshausen-Amundsen	NOAA 85% SIC	68 (39)	**-15.7**	116 (45)	8.2	64 (21)	**-8.7**
	NOAA EASE grid 78% SIC	70 (23)	**-11.8**	111 (30)	4.8	73 (16)	**-7.2**
	OSISAF 75% SIC	64 (42)	**-8.7**	95 (31)	1.7	60 (19)	**-9.4**
	OSISAF EASE grid 75% SIC	59 (45)	**-15.1**	96 (29)	2.5	61 (20)	**-8.4**
	JRA-CESM 85% SIC	1 (2)	0	99 (66)	0.5	12 (6)	-0.2
	JRA-CESM 0.4m SIT	9 (15)	0	26 (24)	2.6	33 (15)	0.7
Weddell	NOAA 85% SIC	27 (14)	**-2.6**	249 (260)	-17	51 (22)	0.5
	NOAA EASE grid 78% SIC	48 (11)	**-3.1**	164 (118)	**-16.3**	58 (13)	-1.8
	OSISAF 75% SIC	52 (9)	0	129 (130)	**-18.9**	54 (12)	-1.6
	OSISAF EASE grid 75% SIC	40 (13)	-2.9	145 (108)	**-22.1**	50 (10)	-1.4
	JRA-CESM 85% SIC	49 (42)	4	225 (223)	-30	87 (23)	-4.3
	JRA-CESM 0.4m SIT	33 (24)	-4.3	120 (63)	-14.3	62 (21)	-4.8
Indian	NOAA 85% SIC	54 (19)	0.1	97 (76)	1.1	45 (9)	0.8
	NOAA EASE grid 78% SIC	59 (15)	0.9	114 (29)	-3.1	48 (7)	1.4
	OSISAF 75% SIC	44 (9)	2.3	134 (53)	-0.4	42 (6)	-0.5
	OSISAF EASE grid 75% SIC	56 (12)	0.8	112 (31)	-2.8	47 (8)	0
	JRA-CESM 85% SIC	21 (13)	**-4.1**	167 (132)	-16.2	45 (14)	**-3.8**
	JRA-CESM 0.4m SIT	84 (31)	**-9.6**	191 (61)	5	69 (14)	-1.3
Pacific	NOAA 85% SIC	107 (30)	5.7	58 (37)	9	58 (11)	**4.9**
	NOAA EASE grid 78% SIC	87 (18)	2.9	80 (19)	0.7	57 (7)	**2.6**

	OSISAF 75% SIC	68 (17)	-3.5	89 (36)	3.9	46 (8)	0.4
	OSISAF EASE grid 75% SIC	74 (17)	-1.2	76 (18)	3.1	51 (9)	1.2
	JRA-CESM 85% SIC	0.1 (0.5)	0	72 (46)	-7.8	16 (5)	0.5
	JRA-CESM 0.4m SIT	97 (25)	-3.2	134 (58)	1.6	59 (8)	0

Table 2. Linear trends in regional monthly polynya area. Trends are in units 10^3 km^2/decade. Products and thresholds are calculated using products on the CESM nominal 1° grid and monthly data except where otherwise specified. Bold text indicates trends that are at 95% or higher significance based on the Mann-Kendall non-parametric significance test (Mann 1945, Kendall 1975, Gilbert 1987). Dashed lines indicate region and season when no polynyas were identified using that product and metric at least 1/3 of the months in the timeseries.

4.3 Polynyas in the JRA-CESM vs NOAA and OSISAF OBS

4.3.1 Integrated southern hemisphere polynya area

Polynya-like features have been found in CESM2 (DuVivier et al., 2021; Singh et al., 2020), and the CESM2 reproduces many characteristics of Antarctic sea ice quite well, making it a suitable model for closer investigation of polynya-like features. Polynyas identified in the model and the observations may disagree if the model doesn't adequately capture mechanisms for producing polynyas or due to model bias. It is also possible that identification of polynyas in model output may require different metric choices than those used to identify polynyas in satellite products due to differences in model vs satellite data as outlined above.

Variability in SH polynya areas tends to be larger during the ice retreat season November-January) in both OBS and the JRA-CESM, and SH polynya area for a given SIT threshold value are largest in November (Fig. 3b and Supplemental Figs. 3-4). Polynya maps for the example day, July 15, 2003, show how the 85% SIC threshold identifies far fewer polynyas in the JRA-CESM than either the NOAA or the OSISAF CDRs (Fig. 2), suggesting that SIC may not identify polynya-like features in model output in the winter season. Indeed, monthly climatological (1979-2020) SH polynya areas remain very small in the JRA-CESM across the full range of SIC thresholds for fall through mid-winter (April-July; Fig. 3e and Supplemental Fig. 5). During freeze up through winter, open water can freeze very quickly in the model, resulting in high SICs and yet relatively thin SITs. Monthly climatologies of SH polynya area reveal that SIT thresholds identify large areas of polynyas throughout the fall and winter across a range of SIT thresholds, unlike SIC thresholds (Fig. 3e and Supplemental Fig. 5). Comparing polynyas identified in the satellite observations and the model output, we find that on a climatological, hemispheric basis, the best correspondence between SH polynya areas identified in the model and the observations differ by month: model simulated polynya areas identified using a 0.4 m SIT threshold correspond well to the observations in late fall through early spring (April-October), whereas SIC of 85% in the model output for late spring months (November) more closely correspond to those from the satellite product. Variability in the SH polynya area is highest in December and January (Supplemental Figs. 3-5), when Antarctic sea ice is rapidly retreating (Fig. 1e). The smallest polynya areas across all thresholds in the JRA-CESM, as in the CDRs, are found in February and March, when sea ice is at a minimum then beginning its seasonal expansion.

The metrics and thresholds that identify similar integrated SH polynya areas in the JRA-CESM to observationally based estimates are a SIT of 0.4 m and SIC of 85%. Figure 4 shows time series of SH polynya area and total number of SH polynyas for July and November and underscores many of the complications comparing polynyas estimated from satellite products to those estimated using climate model output on a seasonal basis. There are significant seasonal differences in polynyas identified using these metrics: polynya areas identified using the SIT metric are roughly three times as large as those identified using the SIC metric (and much closer to the SH polynya areas in both OSISAF and NOAA CDRs) for spring-winter (Figure 3, Table 1 and Supplemental Figure 6), whereas the magnitude of SH polynya area is similar using both SIT and SIC metrics in the model output for the spring. Interestingly, the mean and variabilities in November SH polynya areas in the JRA-CESM identified using SIC more closely match those in the NOAA timeseries than those using the SIT, which more closely match the mean and variability in the OSISAF SH polynyas (Figures 4-5, Table 1 and Supplemental Figure 6).

Temporal correlations for SH polynya area, 1979-2020, between the monthly OBS and JRA-CESM are significant for only a few months of the year – namely July-October using the 0.4m SIT threshold for the NOAA timeseries, and the months of April (SIT 0.4m), August (SIT 0.4m) and September (SIT 0.4 m, SIC 85%) for the OSISAF timeseries (Figure 5e). On an annual basis, correlations are positive and significant with both OBS however only for the SIC threshold in the JRA-CESM. Correlations between SH polynya timeseries in July/August between the SIT-based JRA-CESM polynyas and the NOAA CDR (R=0.59/0.48) are nearly as high as the correlations between the monthly OBS (NOAA-OSISAF; R=0.69/0.60). The number of discrete polynyas identified in the satellite products are 2-3 times as numerous as those identified in the model output, and thus larger, except during the summer months (DJF) when the number of discrete polynyas in the OSISAF and the JRA-CESM using SIT as a metric are similar ((Figure 5, Table 1 and Supplemental Figure 6). Thus, polynyas in the JRA-CESM tend to be large. Correlations between the two different polynya timeseries from the JRA-CESM (SIC at 85% threshold and SIT at 0.4 m threshold) vary widely from month to month and are statistically significant and positive for about half of the months (March, July- Oct and on an annual basis) while in other months the correlation is close to zero (Fig. 5c). Trends (1979-2020) in SH polynya areas in the JRA-CESM are negative, as they are in the OBS, however they are significant only in the SIT in July-August, and in both SIT and SIC derived timeseries on an annual basis.

4.3.2 Regional polynya areas

Polynyas in the Bellingshausen-Amundsen sea region tend to be anemic compared to the OBS in winter (July), with the possible exception of polynyas identified using the daily SIT metric. In contrast, in spring (November) the SIC threshold identifies higher modeled polynya areas in this region and they are closer to the polynya areas identified in the NOAA and OSISAF. The monthly 0.4 m SIT threshold identifies larger areas of polynyas in the Pacific than those identified in the satellite product for July, however in November the SIC 85% threshold results in larger polynya areas in this region. In general, the

spatial correlations between polynya area as a function of longitude identified in the satellite products and the JRA-CESM polynya area (Fig. 7) are higher than the temporal correlations for the integrated SH timeseries (Fig. 5). Thickness based polynyas in the JRA-CESM are significantly correlated in longitude with both OSISAF and NOAA polynyas for all months of the year, and concentration based polynyas are significantly correlated with those identified in both OBS all months except April (OSISAF), May-July (NOAA), and September-October (OSISAF). Correlations with JRA-CESM tend to be higher for the NOAA CDR and SIT-based polynyas for most although not all months and annually (Figure 7).

Monthly and annual correlations between timeseries of regional polynya areas highlight further complexities when comparing polynyas identified with different metrics and data products. Regionally, significant temporal correlations occur ~25% (9%) of the time between the SIT 0.4m (SIC 85%) threshold and the NOAA CDR, and 15% of the time for the OSISAF CDR – yet only 7-9% of the time for the SIC-identified polynyas in the JRA-CESM. Most of the significant correlations between the model and the observations occur in the Ross Sea between the NOAA and SIT-identified polynyas in the JRA-CESM (Figure 8 and Supplemental Figures 7-11). In general, polynyas identified in the JRA-CESM have higher spatial correlations (w.r.t. longitude) than temporal ones (SH or regional) with the polynyas estimated in both OBS, even though the model identifies polynya areas of similar magnitude and variability as seen in the OBS (using either or both of the SIT/SIC metrics) often captures the mean and variance both hemispherically and regionally (Tables 1,2).

Integrated polynya areas in the JRA-CESM from both SIC and SIT thresholds are significantly correlated with each other ~32% of the months/annual basis over the five regions, most consistently in the late winter/early spring, with the exception of the Pacific sector where they are not significantly correlated (Figure 8). By November, when simulated Antarctic sea ice begins its spring retreat (e.g. Fig. 1e) and is losing volume more rapidly than extent (SH sea ice loses 22%/18% of its annual extent loss and 33%/30% of its annual volume loss in November for the JRA/CESM2; not shown), correlations between polynyas using SIT and SIC thresholds become either less highly correlated (Ross, Bellingshausen-Amundsen Seas) or are not significantly correlated (Figure 8). The generally insignificant spring through winter (April-August) correlations between coastal polynya areas identified using in the JRA-CESM using the SIT and SIC may be at least partially due to the very low polynya areas identified by SICs when air temperatures lead to rapidly forming sea ice and high SICs even in very low SIT regions. The exception is the Weddell Sea - where winter polynyas identified using both metrics are similar in mean and variability (Figure 8, Table 2).

Regional trends are quite varied in sign, magnitude and season across all data sources (Table 2 and Supplemental Figures 7-11). Regional polynya area trends (1979-2020) are insignificant for most months in both the SIT and SIC identified regional JRA-CESM timeseries, with a few exceptions. Trends are significant and negative in the Indian sector in July (SIT and SIC metrics) and on an annual basis using the SIC metric. Significant regional trends are found in both of the OBS and one of the JRA-CESM polynya timeseries (SIT or SIC) for only two regions and months – in the Ross Sea in March (Supplemental

Figure 11), and the Pacific Sector in October (Supplemental Figure 10). Although all three polynya timeseries (NOAA, OSISAF, and JRA-CESM using SIT) show significant negative March trends in the Ross Sea, two show significant positive (NOAA and JRA-CESM using SIC) and the other significant negative (OSISAF) October trends in the Pacific Sector. In August in the Indian sector, however, both JRA-CESM polynya timeseries have significant negative trends, whereas the NOAA polynyas have significant positive trends, and the OSISAF do not have significant trends. One possible source of differences in trends between the hindcast model output and the satellite-based products may lie in the reanalysis product used to force the CESM-JRA, discussed in section 5 below, although differences in trends between the OBS also suggest high uncertainties in many regional polynya trends.

4.4 Impacts of different definitions for sea ice concentrations in the model and satellite data

Discrepancies between wintertime polynya identification using SIC in the model and the OBS data may arise due to differences in SIC definitions in satellite-based versus model data. As discussed above, sea ice can form immediately in the model during the cold austral expansion season and through the winter, thus resulting in SICs that are high even though the ice may be very thin. Satellite imagery cannot differentiate between water and sea ice at very low SICs or low sea ice thicknesses. To understand potential impacts that these model and observational differences in SICs may have in polynya identification metrics, we degrade the model SIC output to more closely mimic satellite estimates of SIC. In areas of low (<10% SIC) or thin (<5cm SIT) ice, we set daily SICs to 0% SIC, and in thin ice areas (5-20 cm SIT) the originally modeled SICs are reduced by half. We then identify polynyas using an 85% SIC threshold on the degraded model output.

Comparisons of the standard model to degraded output indicate that degrading SICs results in small differences that are largest within the ice pack during ice growth season and along the ice edge in the winter (Appendix C and Supplemental Figs. 4-5); differences from degraded output during the sea ice retreat season (OND) are much smaller with no discernible patterns (not shown). Degrading the model data results in lower SICs throughout much of the fall pack ice and along the winter sea ice edge, and these differences show very little regional variability and do not consistently explain the model bias of the non-degraded data compared with the satellite product and in some cases would further increase model-observational biases (Supplemental Figs. 4-5). Identifying polynyas based on the degraded model data (using an 85% SIC threshold) results in an increase in fall and wintertime polynyas by ~10-20% (Figure 4 and Supplemental Figures 12-13). This increase is quite small compared to the model versus CDR polynya area differences. Thus, it does not explain the differences in polynya areas estimated from these three products and we focus on results using the standard model output (non-degraded) for the remainder of this paper.

4.5 Relationships between polynyas and NPP in the JRA-CESM

Net primary productivity (NPP) describes the rate of photosynthetically fixed carbon in the upper ocean; it quantifies the energy available for marine food webs. In the high-latitude Southern Ocean, NPP increases markedly as the sea ice retreats and light returns to Antarctic waters (e.g. Richert et al., 2019 and references therein). Light reaches the surface sooner in

polynyas than the surrounding ice-covered areas, relieving phytoplankton of light limitation (e.g. Arrigo & van Dijken, 2003). We look at polynya regions defined in the austral spring (September, October, November, "SON"), to see if the model captures high NPPs within identified polynyas during the early growth season as is found in observations. The choice of metric (concentration or thickness) to identify SON polynyas in the model is not clear based on the previous analysis that indicates not only differences between the two OBS w.r.t. polynya areas, temporal and spatial correlations and trends, but also that polynyas identified in the JRA-CESM using a 0.4 m SIT and 0.85% SIC thresholds each have months or regions that better correlate with the NOAA or with the OSISAF. We therefore use austral spring polynya regions as identified by both the 0.4 SIT and the 85% SIC metrics for the NPP analysis.

Comparing the monthly average NPP per unit area within austral springtime coastal polynyas and within the sea ice zone allows us to better understand how polynyas may augment austral spring NPP and thus play a critical role in the Antarctic food web (Figure 9). Note that the SIZ, which is defined as the area covered seasonally with sea ice (as determined by the mean winter - JJA - 85% SIC contour) covers significantly more ocean area than the spatial area of polynyas, so the overall production within the SIZ is larger than in polynyas (Figure 9, top). However, we find that the NPP per unit area is substantially higher during the austral spring in regions identified as polynyas using both SIC and SIT polynya identification methods than it is within the SIZ generally (Figure 9, bottom). This finding suggests that the model does indeed capture high productivity within low and thinner ice regions. Additionally, the higher NPP per unit area persists into the summer and early spring (December-March) as well. Polynyas have a particularly large impact on NPP during December, when area average NPP within polynyas is more than twice as much as within the SIZ when using the 0.4m SIT threshold and 1.5 higher when using the 85% SIC threshold. Although the total integrated SON polynya area is an order of magnitude smaller than the total SIZ area, NPP within polynyas contributes ~17-23% of the total NPP during the December peak. These results highlight that polynyas are playing an important role in Antarctic marine productivity in the CESM.

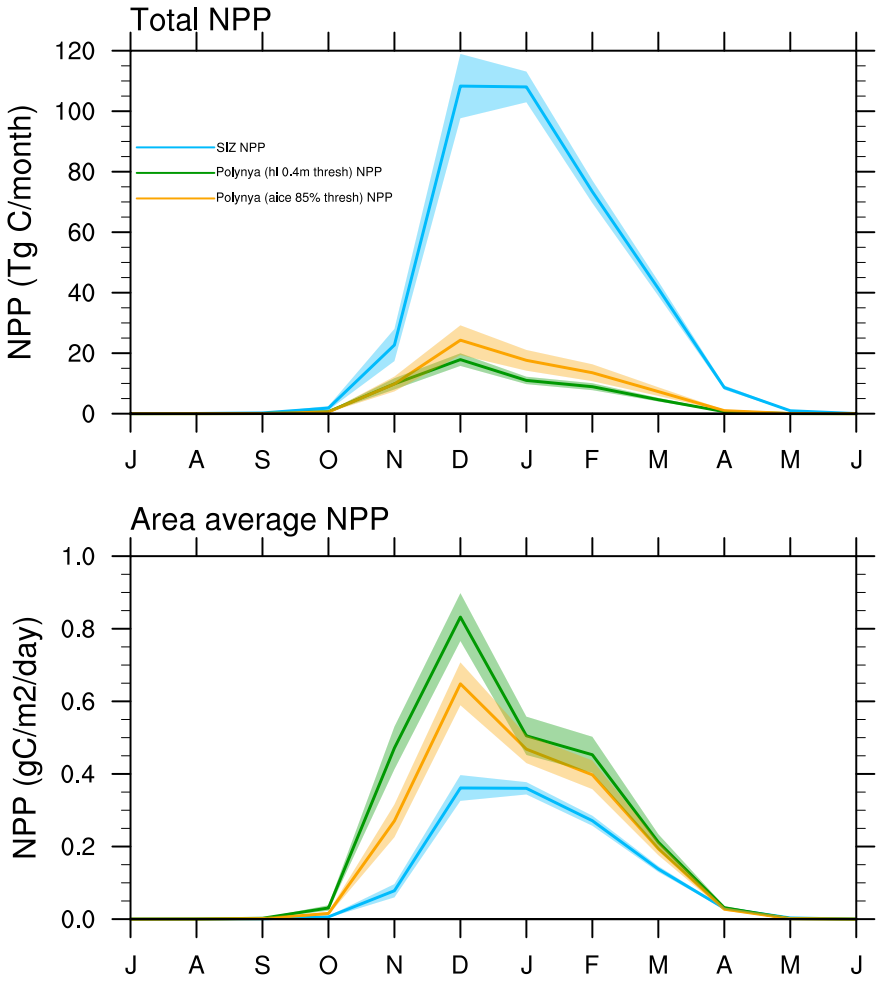

Figure 9. JRA-CESM 1979-2020 climatological integrated SH monthly total NPP (top) and area-averaged NPP (bottom) for the sea ice zone (SIZ: blue) and SON polynya regions identified using 0.4 SIT (green) and 85% SIC (orange) thresholds.

4.6 CESM2-LE: Antarctic coastal polynyas and NPP in a changing climate

The above analysis indicates that the JRA-CESM is simulating polynya-like features with elevated NPP compared to the SIZ. We extend our analysis to the fully-coupled 50 member CESM2 Large Ensemble (CESM2-LE) over the historical (1850-2014) and future moderately-high emission (SSP370) scenario (2015-2100) to explore how polynyas and NPP may change in a changing climate (Figure 10). SH coastal polynya areas identified in the CESM2-LE using both the SIT 0.4m and SIC 85% thresholds indicate that polynya areas tend to be higher in the fully coupled CESM2-LE during July using the SIT threshold, as was found in the JRA-CESM simulations, and the same size in November for both metrics until the mid-1900s, when SH polynya areas identified using SIC start to decline. Simulated polynyas in the hindcast simulation (JRA-CESM) tend to lie on

the high side of the CESM2-LE range and more than 1 standard deviation above the 10-year running ensemble mean for both SIT and SIC thresholds in both July and November, indicating the influence of the reanalysis atmospheric forcing. Polynyas estimated from both OBS fall within the range of the SIT-based July polynyas in the CESM2. In November, NOAA-polynyas lie within the SIC-range, whereas OSISAF polynyas lie within both SIT and SIC identified polynya ranges in the CESM2-LE. The number of discrete wintertime coastal polynyas identified in the observational products is significantly larger than from either polynya metric in the model simulations in July, although in November the numbers of polynyas in the NOAA time series is more closely aligned with polynya numbers in the model (Figure 10). SH CESM2-LE July polynya areas identified using the SIT threshold show small increases from 1850-2100 (Fig. 10a). November SH polynya area decreases in both the SIT- and particularly in the SIC-identified areas over the last 40-50 years of the 21st C (Fig. 10b).

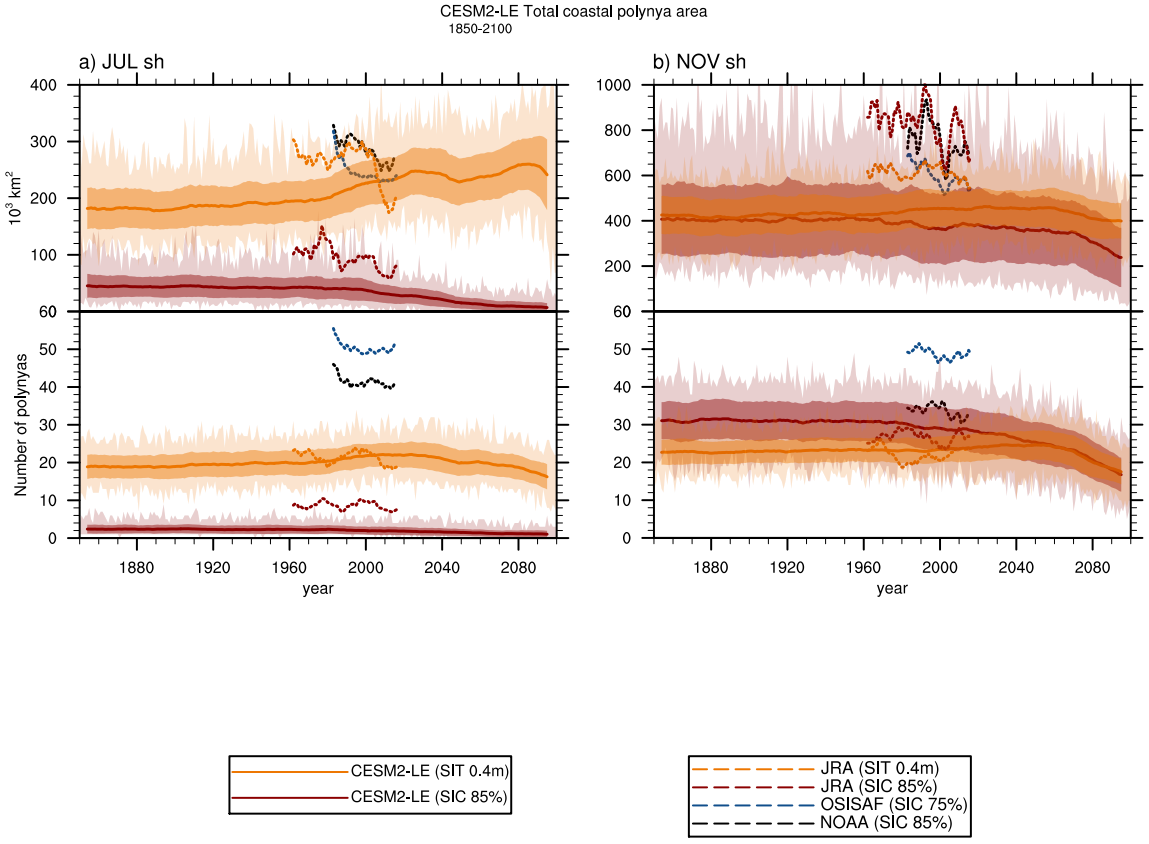

Figure 10. Integrated southern hemisphere mean coastal polynya area and number of polynyas, 1850-2100, for a) July and b) November for the CESM2-LE (SIC 85%, brown; SIT 0.4m, orange), and 1979-2020 (dashed lines) for the NOAA CDR (85% SIC, black), the OSISAF CDR (75% SIC, blue), and the JRA-CESM SIC (SIC 85%, brown; SIT 0.4 m, orange). The CESM2-LE 10-yr running ensemble mean is shown by the thick line, the medium shading indicates ±1 10-yr running ensemble standard deviation, and the light shading indicates the minimum and maximum from the 50-ensemble members.

Trends in springtime (SON) polynya areas show broad similarities to those in July and November, with polynya areas identified using the SIC metric declining starting in the latter half of the 20th century, and those identified using SIT metric increasing until about 2050 then decreasing (Fig. 11d). The differences in trends between polynyas identified using SIT and SIC thresholds may be related to the more rapid decline in sea ice volume compared with sea ice extent in austral spring during the latter half of the 21st century (not shown). SIT associated polynya areas are about 50% higher than the SIC-polynya areas until that latter part of the 20th C, when SIC-associated polynya areas decrease through 2100. SON polynya areas identified using the SIT metric increase from the latter part of the 20th century until the latter half of the 21st century, when they begin to decrease. A more detailed seasonal and regional analysis of these trends along with an exploration of the differences between SIT and SIC metric is beyond the scope of this work.

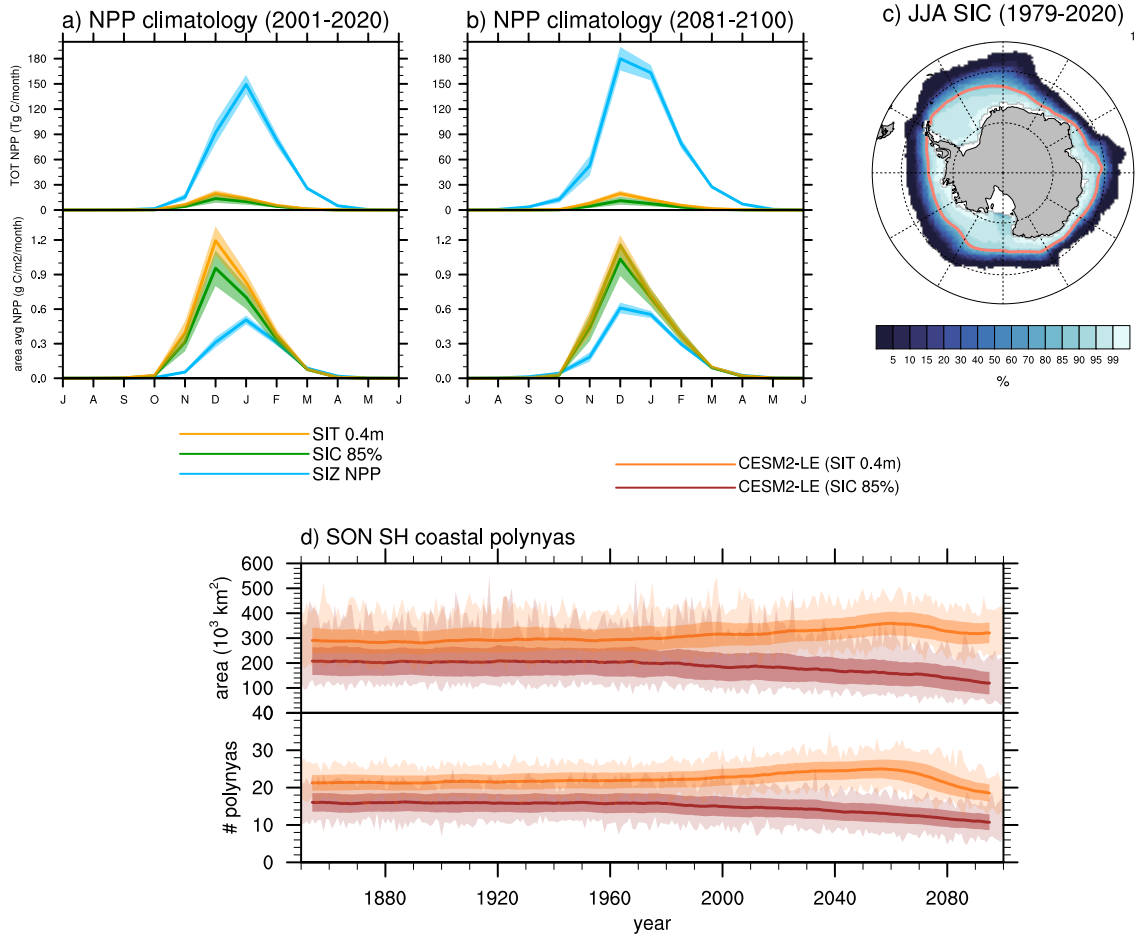

Figure 11. Monthly climatology for total (top) and area average (bottom) NPP for a) first (2001-2020) and b) last (2081-2100) 20 yrs of the 21st Century; c) climatological 1979-2020 winter (JJA) SIC with sea ice zone (SIZ; 85% SIC contour shown in red); and integrated SH spring (SON) d) polynya area (top) and number of polynyas (bottom). NPP is shown within the SIZ (light blue), the SIT-0.4 m polynyas (orange) and the SIC-85% polynyas (green). Solid lines/shading in a-b indicate ensemble mean/±1 standard

deviation. The CESM2-LE 10-yr running ensemble mean SH polynya area and number of polynyas (d, SIC 85%, brown; SIT 0.4m, orange) are shown by the thick line, the medium shading indicates ±1 10-yr running ensemble standard deviation, and the light shading indicates the minimum and maximum from the 50-ensemble members.

As in the JRA-CESM simulation, area average NPP in the CESM2-LE is much higher within polynyas than within the SIZ on a per area basis (Fig. 11a-b). SIZ-NPP in the CESM2-LE peaks in January in 2001-2020, later than the December peak NPP observed in the JRA-CESM. Ensemble mean SIZ-NPP increases markedly in the 21st century under the moderately high emission scenario, particularly in the early growth season (December) and such that there is a distinct December peak in the climatological SIZ-NPP by 2081-2100. In addition to the changing seasonality of NPP in the SIZ, area average SIZ-NPP and total SIZ-NPP increase in the future scenario. Although polynya areas identified using the SIT are higher than those identified using the SIC metric (Fig. 11d), area average NPP becomes higher at the end of the century within the low SIC polynyas during the peak of the spring bloom, with the result that total integrated SIZ NPP is slightly larger (Fig.11a-b). Area average NPP within the polynya areas shows much smaller changes than within the SIZ, with slight increases/decreases within SIT/SIC identified polynyas during the December peak. NPP within polynyas contributes a small portion of the total NPP by the end of the 21st Century (Fig. 11b). Changes in seasonality of the SIZ NPP may be accompanied by changes in efficiency of trophic transfer (i.e. the dominant phytoplankton types may shift, as shown in Krumhardt et al. 2022) – analysis of trophic level changes in a changing climate are left for future analysis.

5 Discussion

Polynyas are often qualitatively defined -- “open water surrounded by ice and/or ice and land” -- and a leading conclusion of this work is that care must be taken when identifying polynyas quantitatively from gridded data. Polynyas are a feature of the sea icescape – a complex, dynamically changing structure that is an integrated component of polar marine ecosystems as well as a leading player in polar oceanic and atmospheric circulations and dynamics. Ideal metrics and thresholds for polynya identification will depend on the product grid sizes, region of interest, season and scientific application, as well as the specifications of an individual data product.

Sea ice concentrations retrieved from satellite images reveal much about the sea icescape, but areas of low SICs and/or low SITs such as polynyas are difficult to capture through remote sensing. Polynya areas identified in both OBS are significantly correlated spatially (longitudinally) for all months and annually, regardless of spatial (EASE vs model) and temporal grids (daily vs monthly), however R values are relatively low (~0.5) for April through October considering both the OBS use the same base data and differ only by retrieval algorithm. Temporally integrated SH polynya areas are significantly correlated, although with lower R values in general than the spatial correlations. This is true both within an OBS (e.g. NOAA EASE: NOAA regridded) and between the OBS (NOAA:OSISAF) for all months and grids, except for April and October. Differences

in polynyas identified in the two OBS suggest a sea icescape complexity that may not be fully captured by SIC retrieved from satellite imagery.

Differences in the satellite-based OBS present challenges in comparing polynyas identified in a model with those identified in observationally-based products. Spatial (longitudinal) correlations between the JRA-CESM (SIT) and NOAA polynyas from April-October are nearly as large as they are between the observational products, and the JRA-CESM SH polynya area (based on SIT metric) is significantly correlated with the OSISAF/NOAA in April/October. Results from the JRA-CESM indicate that the model is successfully simulating polynya-like features in the icescape along the Antarctic coast, in a manner that is spatially consistent with the NOAA CDR. The JRA-CESM tends to simulate lower polynya areas in the Bellingshausen-Amundsen sea than those estimated from the either the NOAA or OSISAF products. JRA-CESM indicates that marine NPP, on average, is approximately twice as high within polynya areas as within the sea ice zone as a whole. NPP within polynyas in the JRA-CESM contributes to about 18% of the total Antarctic SH marine NPP even though the sea ice zone is roughly ten times as large as the springtime coastal polynya areas.

The fully coupled CESM also has polynya-like features with relatively high NPP. Integrated polynya area in the CESM2-LE tends to be lower, on average, than in the JRA-CESM, 1979-2020, although the polynya area in the JRA-CESM fall within the spread shown by CESM2-LE during the historical period. NPP within polynyas remains high and relatively unchanged over the 21st century in the CESM2-LE under the SSP370 emissions scenario, although the contribution of NPP within polynyas to the total SH NPP is lower by 2100 primarily due to overall increases of NPP in the sea ice zone.

We provide some “best practices” from this systematic comparison of polynya identification methods in satellite-based and the CESM below, and discuss the implications of polynya metric choices for applications in climate models.

5.1 Polynya metric choices: Temporal and spatial resolutions

Analysis of polynyas identified in both satellite and model products suggest that integrated SH climatologies made from daily vs monthly data do not differ significantly, and thus monthly data may be sufficient for many analyses both from observations and climate model output on larger temporal scales. In general, polynya areas defined by the same SIC threshold and product will be slightly larger using daily data than monthly data for the NOAA CDR. There are seasons and regions, however, that show significant differences in polynya areas between daily data and monthly data at the same threshold value in different data products, and when monthly data may lead to larger polynya area identification – e.g. in the Ross and Weddell Seas from late spring through late summer (November-March). Daily SIT data in the model, however, leads to higher polynya areas than monthly data in the Ross and Bellingshausen-Amundsen seas.

Grid resolution significantly impacts polynya metric and threshold choices and a given threshold value will lead to significantly larger polynya areas on a higher resolution grid than on a lower resolution grid. A constant SIC metric results in different areas of polynyas when used on an equal area grid than on a equal-degree grid (e.g. Appendix), which may explain our differing results in trends seen from polynya areas identified in the OBS on the EASE vs 1° grid. In order to eliminate discrepancies due to grid types and resolutions alone, we recommend comparing metrics from data on the same grid, and regridding - if necessary - data with the higher geographical resolution onto the lower resolution grid.

5.2 Polynya product and metric choice in modeled data

Using SICs, in general, to identify SH wintertime coastal polynyas in model simulations requires very high thresholds and is particularly problematic in the Bellingshausen-Amundsen Sea. Part of this issue is likely because ocean surface waters can very rapidly refreeze and form very high sea ice concentrations in all models, not just the CESM. Degrading model output to more closely resemble satellite estimates of SICs leads to only small increases in polynya areas identified using SICs (at 85% threshold) and does not explain the large bias between polynyas identified in July by the OBS and JRA-CESM using 85% SIC thresholds. A more direct comparison between SICs as a metric to identify polynyas in both simulated and observed data could be made with the use of a satellite-simulator in the model to calculate brightness temperatures as a satellite would measure them (e.g. Smith et al., 2021). Wintertime polynya-like features are identified in the CESM using daily SICs along the eastern Antarctic coast, and yet not in the Bellingshausen Sea (e.g. Fig. 4) suggesting that there may be model biases in the CESM impacting regional sea ice dynamics.

While SIT is not available in long term satellite observations as an identification metric, SITs readily identify wintertime polynya areas in models across a range of thresholds and for all regions. SITs continue to successfully identify modeled polynyas as the ice begins its retreat in September-October, although by November, SICs identify polynya areas in the model output across a range of thresholds and of similar magnitudes as found in both of the regridded OBS data. This study assesses only the CESM2 model, and more work should be done to test if the seasonality of SIC and SIT as a polynya identification threshold differs by model. Polynyas identified in the model output are significantly correlated geographically for both SIC and SIT thresholds with those estimated from both the NOAA and OSISAF CDR data in November. We thus find that identification of wintertime polynyas in the CESM better reproduces observed polynyas when using a SIT-based threshold, which more accurately accounts for low sea ice areas than SICs, which can be very high in the model even in very thin sea ice conditions, unlike in satellite imagery. We suggest using a SIT-based metric for winter-time polynya identifications in model output. SITs continue to serve as a good metric for polynya identification in model output in the early spring when sea ice is still quite extensive, although SIC metrics tend to perform better as the sea ice thins and sea ice extent begins a rapid retreat - which is in November in the CESM but may differ somewhat in timing in other models (e.g. Roach et al., 2020). We recommend considering both SIC and SIT based metrics for polynya identification in the austral spring.

It is interesting to note that while significant longitudinal correlations exist between polynya areas identified in the CESM-JRA and the OBS for each month of the year and annually (Fig. 4c), the same cannot be said for temporal correlations of the integrated time series (Figs. 5c and 6a-e). This suggests that the regionality of the identified polynyas in the CESM-JRA is captured well compared to the observations, however the temporal variability is less well captured in some regions and seasons. Part of this may be explained by the reanalysis data used to force the CESM-JRA and the nature of coastal polynyas. Reanalysis wind products show the lowest biases compared with weather station data in regions and times of high synoptic and/or low katabatic wind activity, and significant biases in wind fields close to the coast near where katabatic winds significantly impact coastal winds (e.g. Jones et al., 2016; Harrison et al., 2022). Katabatic winds are integral to the formation of coastal polynyas (e.g. Thompson et al., 2020 and references therein). Thus, coastal polynya variability due to variability in katabatic winds may be captured by the polynya time series in the observations but not well represented in the atmospheric reanalysis data used to force the model.

Recent work found significant positive trends in annual polynya areas in the Ross, Weddell, Indian and Pacific sectors estimated using daily data from the OSISAF CDR product at a 50% threshold on the 25 km x 25 km EASE grid (Duffy et al., 2023). Our results show significant positive polynya area trends in the OSISAF only in the summertime (DJF) in the Weddell Sea, summer (December) and fall (MAM) in the Indian sector, and summer-fall (DJFMAM) in the Pacific sector, and significant negative trends in the Bellingshausen-Amundsen Sea (Jan-Sept), the Weddell Sea (April-May; Oct-Nov), the Indian sector (Oct), the Pacific sector (Aug-Sept) and Ross Sea (April-November). These contradictions may be due to differences in metrics or methods used to identify polynyas - an analysis beyond the scope of this work - yet it highlights that caution should be taken when comparing results from different sources, grids, methods and metrics.

5.3 Polynya applications: polynyas and NPP in a changing climate

Our analysis with the CESM2-LE demonstrates using a 0.4 m SIT and an 85% SIC metric to identify polynyas in the austral spring (SON) result in larger ensemble mean areas of polynyas in the SIT-identified polynyas than in the SIC-identified ones. Contributions to NPP are quite similar in both SIC and SIT-defined polynyas, and polynyas identified using both metrics show substantial augmentation of Antarctic NPP within polynyas compared to within the entire SIZ, indicating that the CESM is indeed capturing enhanced productivity within polynya-like features in austral spring. Changes in NPP within polynyas are small compared to those within the SIZ, which increases substantially and changes seasonality by the end of the 21st Century. This analysis demonstrates that the CESM may be a useful tool to investigate changing Antarctic marine ecosystems within polynyas and the sea ice zone in a warming climate. As the climate warms and sea ice responds, better understanding how to identify polynyas in different regions or seasons will be critical for quantifying how production in the ocean around Antarctica may change including timing of peak NPP production, changes in trophic transfer and species composition, etc.

6 Conclusions

The definition of "polynyas" in a quantifiable sense is relatively subjective. Defining areas and timing of open water within the Antarctic sea ice zone such that comparisons can be made between satellite based SICs and model output require careful consideration and recognition of the basic differences between satellite observations and model output. It is critical to consider grid type and resolution, season, metric and threshold as optimal metrics chosen may depend on region and season of interest. Our six primary recommendations are:

1) all data should be regridded to the same type and size of grid for comparisons to reduce differences due to grids alone
2) polynya areas identified from monthly and daily data are comparable on annually averaged, integrated hemispheric basis
3) sea ice thicknesses are a more suitable metric for identifying polynyas in climate model data in the winter months
4) sea ice concentrations are a more suitable metric for identifying polynyas in the late spring in climate model data, when sea ice is rapidly retreating, though this may be model dependent
5) optimal metric and threshold choices will be influenced by grids, regions, and seasons of interest
6) productivity within polynya areas may help evaluate model performance with respect to capturing enhanced productivity in polynya-like features, as seen in observations.

Appendices

Appendix A: Polynya algorithm

The polynya algorithm cycles through maps of the sea ice variable (concentration or thickness in this work) and initially labels any grid cells that fall below the threshold and that lie within the sea ice zone (south of the open ocean boundary). The algorithm iteratively cycles through the polynya maps to determine if grid cells that meet the threshold criteria are surrounded by sea ice and land (in which case they are labeled a polynya) or lie next to open ocean (in which case they are not identified as a polynya). Figure AA1 shows a schematic of a hypothetical region with land, ocean, sea ice and polynya grid cells. In this example, there are two polynyas – one open water polynya (occupied by three grid cells), and one coastal polynya (occupied by two grid cells). Figure AA2 shows an example satellite image of the Ross Bay and Terra Nova polynyas and grid cells labeled by SICs.

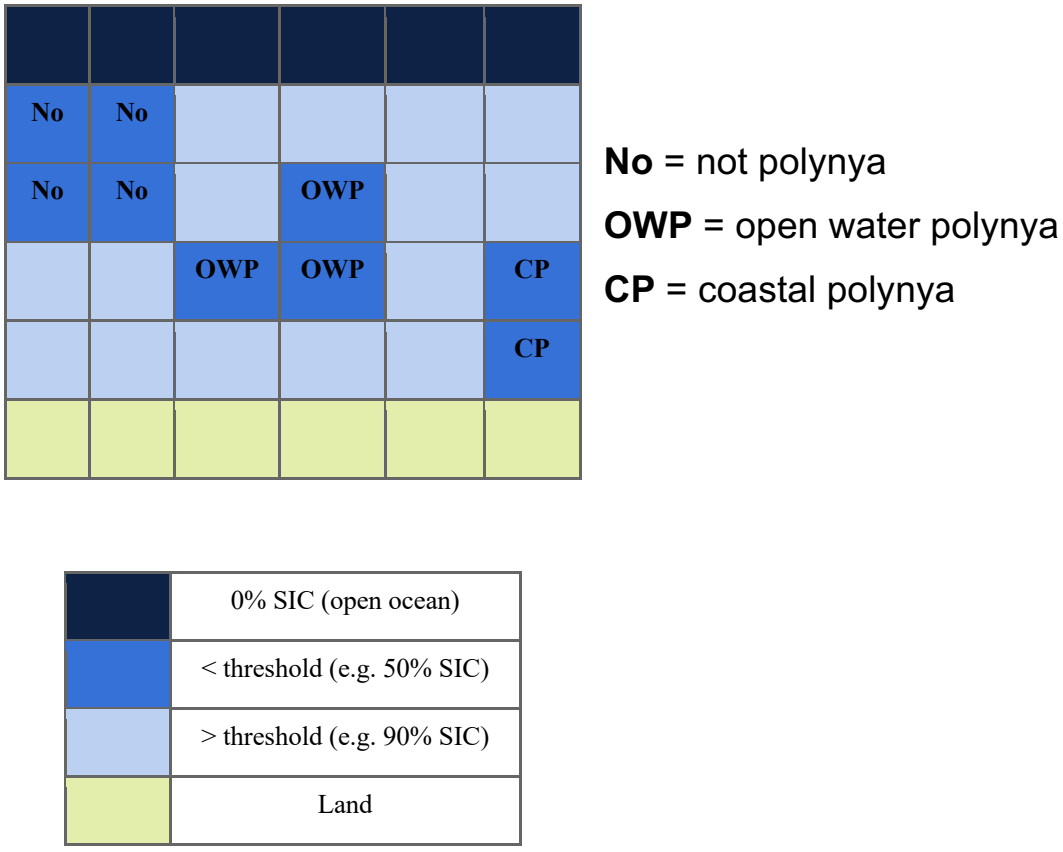

Figure A1. Schematic of grid cells considered open ocean (dark blue), land (light green) and within the sea ice zone (light and medium blue). Grid cells in the sea ice zone that meet the threshold criteria are in medium blue; grid cells that lie above the threshold are in light blue. Grid cells that meet the criteria are identified as polynyas only if they are bounded by sea ice (open water polynyas) or sea ice and land (coastal polynyas).

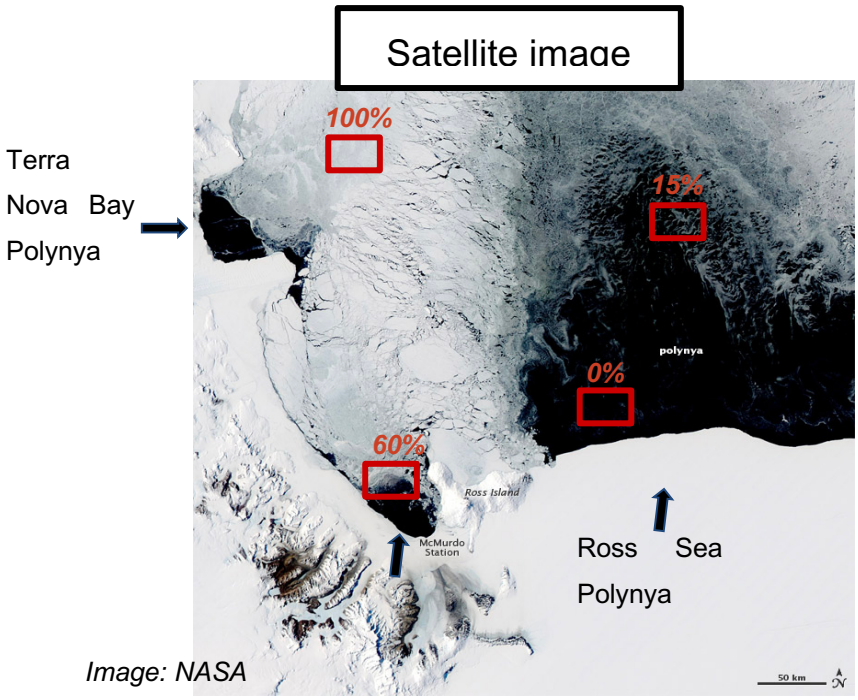

Figure A2. Example satellite image of the Terra Nova Bay and Ross Sea polynyas (Moderate Resolution Imaging Spectroradiometer (MODIS) image of the day from the National Aeronatics and Space Administration (NASA) Aqua satellite, November 16, 2011 https://eoimages.gsfc.nasa.gov/images/imagerecords/76000/76474/rosssea_amo_2011320_lrg.jpg). Hypothetical grid cells with SICs are shown in red.

Appendix B: Grid size and type and impact on polynya definitions

Using concentration thresholds to define polynya regions will define how much open water (or sea ice) is in the grid cell by percentage. For an Equal Area Scaleable Earth (EASE) grid this will correspond to an area that doesn't change with latitude or longitude, whereas on an equal latitude-longituide grid a SIC percent threshold will correspond to different areas of open water (or sea ice) depending on latitude. For example, a 50% sea ice concentration threshold on a 25kmx25km EASE grid corresponds to 312.5 km^2 or more of open water (and also 312.5 km^2 of sea ice) within the grid cell to meet the threshold requirement for a polynya. A grid based on latitude and longitude, which is common for earth system models, will have a varying range of surface area in each grid cell. Figure AB1 shows the sea ice concentration at which a grid cell on the CESM grid (~1°x1° lat/long) will contain 312.5 km^2 of open water, or the same area of open water as on a grid cell on an EASE grid that has 50% SIC. An example of the SIC thresholds required to result in 312.5 km^2 of open water within a grid are shown in Fig. AB2 for an equal area grid cell and two grid cells from a 1°x1° grid cell at two different latitudes. Different grid sizes can also lead to different numbers of polynyas even when the areas are the same (e.g. Fig. AB3).

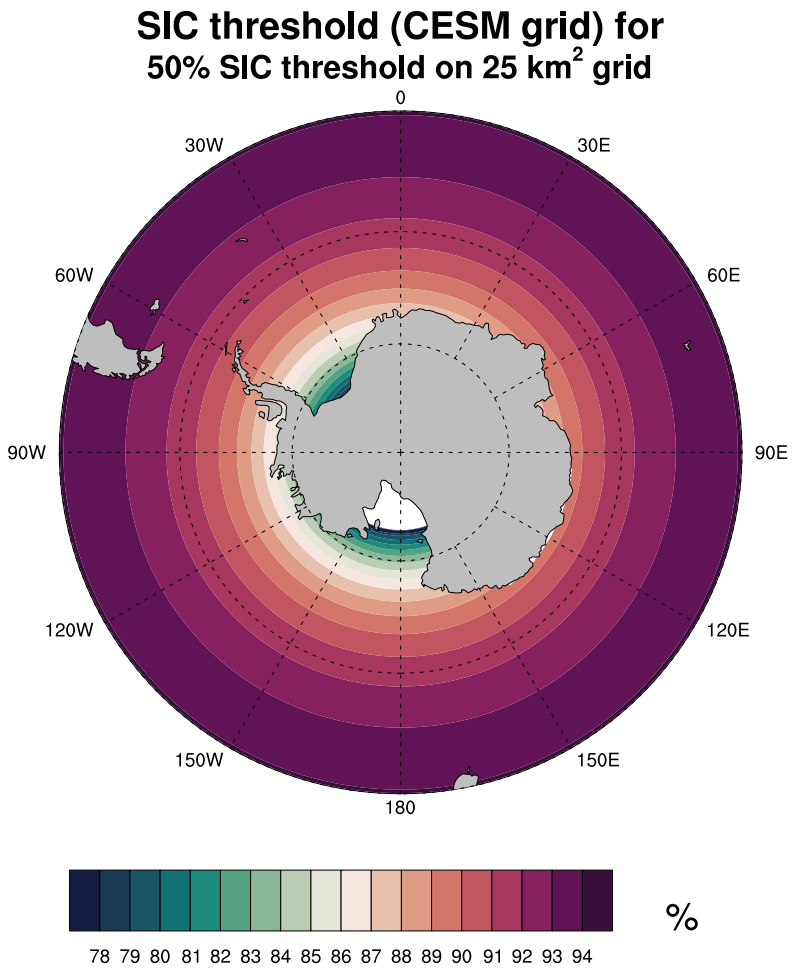

Figure B1. Sea ice concentration required to result in 312.5 km^2 open water within a grid cell on the CESM nominal 1° grid.

895

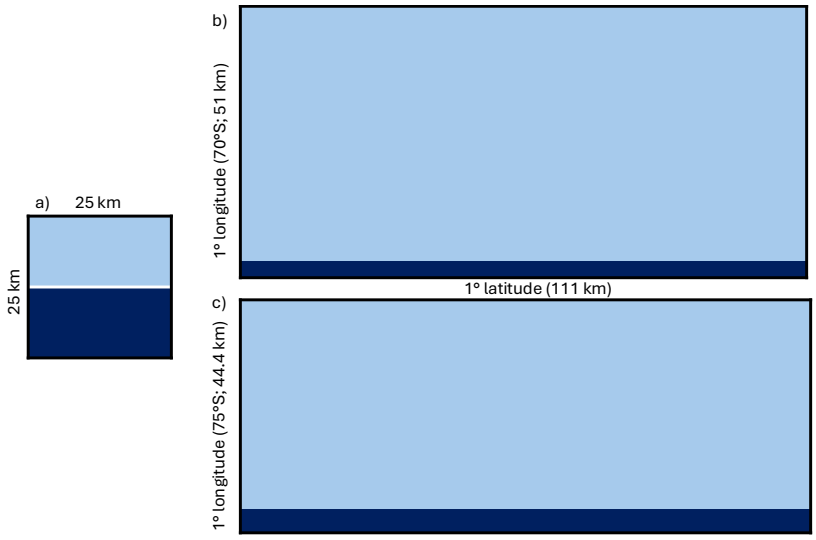

Figure B2. Sea ice concentration required to result in 312.5 km^2 of open water within a grid cell: a) SIC 50% on a 25 km x 25 km equal area grid cell, b) 92% SIC on a 1°x1° lat/lon grid cell at 70°S (approximately 111km x 51km), and c) 84.4% SIC on a 1°x1° lat/lon grid cell at 75°S (approximately 111km x 44.4km)

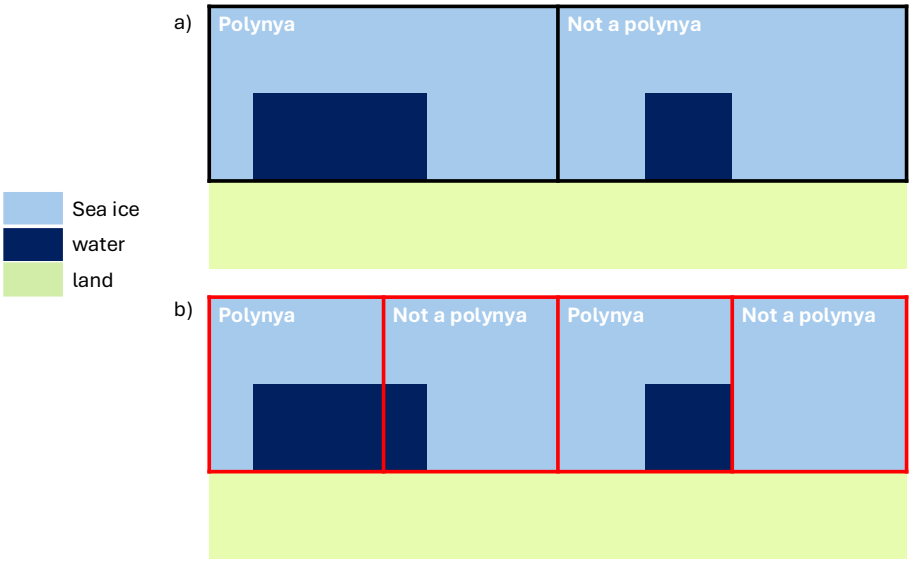

Figure B3. Examples of grid cells classified as polynyas using a 75% SIC threshold on a larger resolution grid (a) and a smaller resolution grid (b). Both figures have the same total integrated polynya area over the region, however there is only one polynya grid cell in (a) and two polynyas in (b).

Appendix C: Degrading climate model daily SIC data.

Figure AC1 shows an example of model SICs that are degraded such that the new sea ice concentrations are set to 0 where the original SICs are less than 10% and also where SITs are less than 5 cm. In regions of SITs that fall between 5cm and 20 cm, SICs are set to half of the original values. The resulting degraded product has noticeably lower SICs along the ice perimeter and isolated locations near the Antarctic continent with lower SICs.

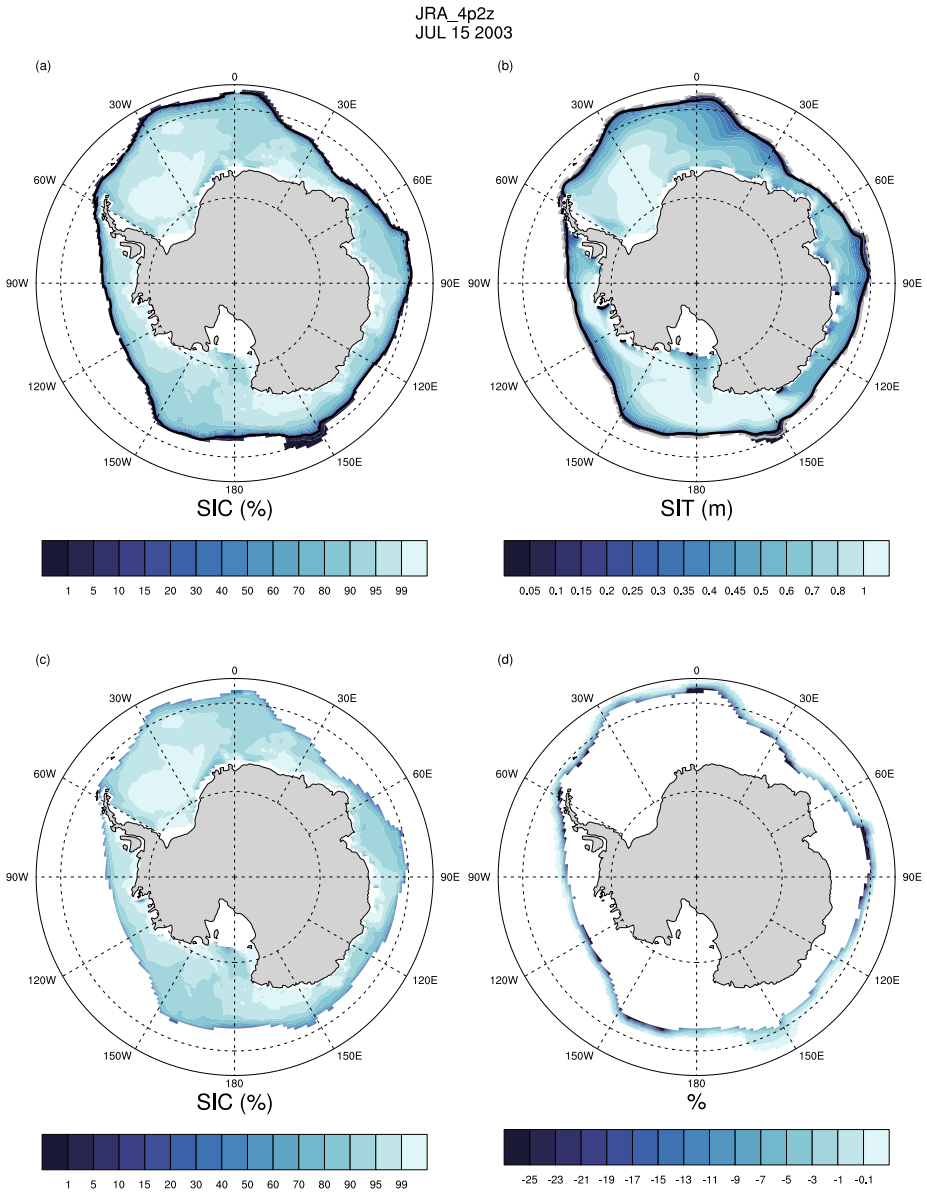

Figure C1. Sea Ice Concentration (a) and sea ice thickness (b) from the JRA-CESM run on July 15, 2003. Degraded sea ice (c) and d) the resulting change in SIC by degrading the sea ice.

Code and data availability

The CESM2-LE data used in this study are freely available, as described in Rodgers et al. (2021). The CESM2-LE and the JRA hindcast simulations (Forced Ocean Sea Ice, FOSI) are freely available from the Earth System Grid

(https://www.earthsystemgrid.org/project/CESM.html). The computational notebooks and other data processing tools used for this publication are freely available online (L.Landrum, 2024). Code for processing the data and making the figures will be published on a GitHub repository in final stages if paper is accepted for publication.

Author contributions

Study design and analysis were conducted by LL with ideas from MMH, AKD, KK and ZS. All authors contributed to the writing of the manuscript.

Competing Interests

The authors declare that they have no conflict of interest.

Acknowledgements

The National Science Foundation (NSF) National Center for Atmospheric Research (NCAR) is sponsored by NSF under cooperative agreement no. 1852977. Previous and current CESM versions are freely available online (at https://www.cesm.ucar.edu/models/cesm2/). The CESM data sets used in this study are freely available online from the NCAR Digital Asset Services Hub (at https://doi.org/10.5065/bgt9-tz46). We thank all the scientists, software engineers, and administrators who contributed to the development and availability of CESM. The CESM project has been supported primarily by the National Science Foundation. We would like to acknowledge high-performance computing support from the Derecho system (doi:10.5065/qx9a-pg09) provided by the Computational and Information Systems Laboratory at NSF NCAR.

We acknowledge support for this work from National Aeronautics and Space Administration (NASA) and the National Science Foundation (NSF) as detailed below. Any opinions, findings, and conclusions or recommendations expressed in this material are those of the authors and do not necessarily reflect the views of these agencies. LL, MMH and KK acknowledge support for this work from the NASA Award 80NSSC20K1289 and the NSF Award 2037531. LL, AKD, KK and ZS acknowledge support for this work from the NASA Award 80NSSC21K1132.

This study has been conducted using OSI SAF Global sea ice concentration climate data record 1978-2020 (v3.0, 2022), OSI-450-a, doi:10.15770/EUM_SAF_OSI_0013. EUMETSAT Ocean and Sea Ice Satellite Application Facility. Data extracted from E. U. Copernicus Marine Service Information: accessed 23 January, 2025.

References

Arrigo, K. R., and G. L. van Dijken, G. L.: Phytoplankton dynamics within 37 Antarctic coastal polynyas, J. Geophys. Res., 108(C8), 3271, doi:10.1029/2002JC001739, 2003.

Comiso, J. C., Cavalieri, D., Parkinson C., and & Gloersen, P.: Passive microwave algorithms for sea ice concentrations: a comparison of two techniques. Remote Sensing of the Environment, 60, 357 384, 1997.

Danabasoglu, G., Lamarque, J. F., Bacmeister, J., Bailey, D. A., DuVivier, A. K., Edwards, J., et al.: The Community Earth System Model version 2 (CESM2). J. Adv. in Model. Earth Sys., 2, 1–35. https://doi.org/10.1029/2019ms001916, 2020.

Duffy, G. A., Montiel, F., A. Purich, A. and C. I. Fraser, C. I.: Emerging long-term trends and interdecadal cycles in Antarctic polynyas, Proc. of the Nat. Acad. of Sc., 121 (11), https://doi.org/10.1073/pnas.2321595121, 2024.

Diamond, R., Sime, L. C., Holmes, C. R., & Schroeder, D. (2024). CMIP6 models rarely simulate Antarctic winter sea-ice anomalies as large as observed in 2023. *Geophysical Research Letters*, **51**(10), e2024GL109265. **https://doi.org/10.1029/2024GL109265**

DuVivier, A. K., Holland, M. M., Landrum, L., Singh, H. A., Bailey, D. A., and Maroon, E. A.: Impacts of sea ice mushy thermodynamics in the Antarctic on the coupled Earth system, Geophys. Res. Lett., 48, e2021GL094287, https://doi.org/10.1029/2021GL094287, 2021.

Eyring, V., Bony, S., Meehl, G. A., Senior, C. A., Stevens, B., Stouffer, R. J., and Taylor, K. E.: Overview of the Coupled Model Intercomparison Project Phase 6 (CMIP6) experimental design and organization. Geosc. Model Devel., 9(5), 1937–1958, https://doi.org/10.5194/gmd-9-1937-2016, 2016.

Fetterer, F., Knowles, K., Meier, W. N., Savoie, M. and Windnagel, A. K.: Sea Ice Index, Version 3. Distributed by National Snow and Ice Data Center, Boulder, Colorado, USA (accessed 2 June 2023); https://doi.org/10.7265/N5K072F8, 2017.

Flores, H., Veyssière, G., Castellani, G. *et al.*: Sea-ice decline could keep zooplankton deeper for longer. Nat. Clim. Chang. 13, 1122–1130, https://doi.org/10.1038/s41558-023-01779-1, 2023.

Fogt, R. L., Sleinkofer, A. M., Raphael, M. N. *et al.:* A regime shift in seasonal total Antarctic sea ice extent in the twentieth century. Nat. Clim. Chang. 12, 54–62, https://doi.org/10.1038/s41558-021-01254-9, 2022.

Gilbert, R. O.: Statistical Methods for Environmental Pollution Monitoring, Wiley, NY, 1987.

Harrison, T. C., Biri, S., Bracegirdle, T. J., King, J. C., Kent, E. C., Vignon, É., and Turner, J.: Reanalysis representation of low-level winds in the Antarctic near-coastal region, Weather Clim. Dynam., 3, 1415–1437, https://doi.org/10.5194/wcd-3-1415-2022, 2022.

Grenfell, T. C., Cavalieri, D. J., Comiso, J. C., Drinkwater, M. R., Onstott, R. G., Rubinstein, I., Steffen, K., and Winebrenner, D. P.: Considerations for microwave remote sensing of thin sea ice, in: Microwave Remote Sensing of Sea Ice, edited by: Carsey, F. D., American Geophysical Union, Washington, D.C., doi:10.1029/GM068p0291, 1992.

Holmes, C. R., Bracegirdle, T. J., Holland, P. R., Stroeve, J., and Wilkinson, J.: Brief communication: New perspectives on the skill of modelled sea ice trends in light of recent Antarctic sea ice loss, The Cryosphere, 18, 5641–5652, https://doi.org/10.5194/tc-18-5641-2024, 2024.

Hobbs, W., and Coauthors, 2024: Observational Evidence for a Regime Shift in Summer Antarctic Sea Ice. *J. Climate*, **37**, 2263–2275, https://doi.org/10.1175/JCLI-D-23-0479.1.

Hunke, E. C., Lipscomb, W. H., Turner, A. K., Jeffery, N., & Elliott, S. (2015). CICE: The Los Alamos Sea Ice Model. Documentation and software user's manual. Version 5.1. T-3 Fluid Dynamics Group, Los Alamos National Laboratory, Tech. Rep. LA-CC-06-012.

Ivanova, N., Pedersen, L. T., Tonboe, R. T., Kern, S., Heygster, G., Lavergne, T., Sorensen, A., Saldo, R., Dybjkaer, G., Brucker, L. and Shokr, M.: Inter-comparison and evaluation of sea ice algorithms: towards further identification of challenges and optimal approach using passive microwave observations, The Cryo., 9, 1797-1817, https://doi.org/10.5194/tc-9-1797-2015, 2015.

Jones, R., Renfrew, I., Orr, A., Webber, B., Holland, D., and Lazzara, M.: Evaluation of four global reanalysis products using in situ observations in the Amundsen Sea Embayment, Antarctica, J. Geophys. Res.-Atmos., 121, 6240–6257, 2016.

Kacimi, S., and Kwok, R.: Arctic snow depth, ice thickness, and volume from ICESat-2 and CryoSat-2: 2018–2021. Geophys. Res. Letts., 49, e2021GL097448. https://doi.org/10.1029/2021GL097448, 2022.

Kendall, M.G.: Rank Correlation Methods, 4th edition, Charles Griffin, London, 1975.

Kern, S., Spreen, G., Kaleschke, L., De La Rosa, S., and Heygster, G.: Polynya Signature Simulation Method polynya area in comparison to AMSR-E 89GHz sea-ice concentrations in the Ross Sea and off the Adélie Coast, Antarctica, for 2002–05: first results, Ann. Glaciol., 46, 409–418, 2007.

Kobayashi ,S., Yukinari, O. T. A., Harada, Y., Ebita, A., Moriya, M., Onoda, H., Onogi, K, Kamahori, H., Kobayashi, C., Miyaoka, K., Takahahi, K.: The JRA-55 reanalysis: general specifications and basic characteristics. J Meteorol Soc Jpn Ser II 93(1), 5–48, https://doi.org/10.2151/jmsj.2015-001, 2015.

Krumhardt K. M., Long, M. C., Sylvester, Z. T. and Petrik, C. M.: Climate drivers of Southern Ocean phytoplankton community composition and potential impacts on higher trophic levels. Front. Mar. Sci. 9:916140. doi: 10.3389/fmars.2022.916140, 2022.

Krumhardt, K. M., Long, M. C., Petrik, C. M., Levy, M., Castruccio, F. S., Lindsay, K., Romashkov, L., Deppenmeier, A.-L., Denéchère, R., Chen, Z., Landrum, L., Danabasoglu, G. and Chang, P.: From nutrients to fish: Impacts of mesoscale processes in a global CESM-FEISTY eddying ocean model framework, Prog. in Ocean., 227, 2024, 103314, ISSN 0079-6611, https://doi.org/10.1016/j.pocean.2024.103314, 2024.

Kwok, R., Comiso, J. C., Martin, S., and Drucker, R.: Ross Sea polynyas: Response of ice concentration retrievals to large areas of thin ice, J. Geophys. Res., 112, C12012, doi:10.1029/2006JC003967, 2007.

Labrousse, S., Fraser, A. D., Sumner, M., Tamura, T., Pinaud, D., Wienecke, B., et al.: Dynamic fine-scale sea icescape shapes adult emperor penguin foraging habitat in East Antarctica. Geophys. Res. Lett. 46, 11206–11218. doi: 10.1029/2019GL084347, 2019.

Lavergne, T., Sørensen, A. M., Kern, S., Tonboe, R., Notz, D., Aaboe, S., Bell, L., Dybkjær, G., Eastwood, S., Gabarro, C., Heygster, G., Killie, M. A., Brandt Kreiner, M., Lavelle, J., Saldo, R., Sandven, S., and Pedersen, L. T.: Version 2 of the EUMETSAT OSI SAF and ESA CCI sea-ice concentration climate data records, The Cryo., 13, 49–78, https://doi.org/10.5194/tc-13-49-2019, 2019.

Li, Y., Ji, R., Jenouvrier, S., Jin, M. and Stroeve, J.: Synchronicity between ice retreat and phytoplankton bloom in circum-Antarctic polynyas, Geophys. Res. Lett., 43, 2086–2093, doi:10.1002/2016GL067937, 2016.

Mann, H.B.:Non-parametric tests against trend, Econometrica 13:163-171, 2045.

Markus, T. and Burns, B. A.: Detection of coastal polynyas with passive microwave data. Ann. Glaciol. , 17, 351- 355, 1993.

Massom, R. A., Harris, P. T., Michael, K. J., and M. J. Potter, M. J.: The distribution and formative processes of latent-heat polynyas in East Antarctica, Ann. Glaciol., 27, 420– 426, 1998.

Meier, W.N.: Comparison of passive microwave ice concentration algorithm retrievals with AVHRR imagery in Arctic peripheral seas. IEEE Trans. Geo. Remote Sensing, 43, 1324-1337, 2005.

Meier, W. N., Peng, G., Scott, D. J., and Savoie, M. H.:. Verification of a new NOAA/NSIDC passive microwave sea-ice concentration climate record. Polar Research, 33. doi: 10.3402/polar.v33.21004, 2014.

Meier, W. N., Fetterer, F., Windnagel, A. K. and Stewart., J. S.: *NOAA/NSIDC Climate Data Record of Passive Microwave Sea Ice Concentration, Version 4*. Southern Hemisphere, 1979-2020. Boulder, Colorado USA. NSIDC: National Snow and Ice Data Center. doi: https://doi.org/10.7265/efmz-2t65, 2021. Accessed June 3, 2023.

Meier, W. N., Windnagel, A., and Stewart, S.: CDR Climate Algorithm and Theoretical Basis Document: Sea Ice Concentration. NOAA NCEI CDR Program, 2021.

Mohrmann, M., Heuzé, C., and Swart, S.: Southern Ocean polynyas in CMIP6 models, The Cryo., 15, 4281–4313, https://doi.org/10.5194/tc-15-4281-2021, 2021.

Nakata, K., Ohshima, K. I., Nihashi, S., Kimura, N., and Tamura, T.: Variability and ice production budget in the Ross Ice Shelf Polynya based on a simplified polynya model and satellite observations, J. of Geophys. Res.: Oceans, 120, 6234–6252, 2015.

Nakata, K.; Ohshima, K.I.; Nihashi, S. Mapping of Active Frazil for Antarctic Coastal Polynyas, With an Estimation of Sea-Ice Production. *Geophys. Res. Lett.*, **48,** e2020GL091353, 2021.

Nihashi, S. and Ohshima, K. J.: Circumpolar Mapping of Antarctic Coastal Polynyas and Landfast Sea Ice: Relationship and Variability, J. Clim, 28, 3650-3670, DOI: 10.1175/JCLI-D-14-00369.1, 2015.

Notz, D.: Sea-ice extent and its trend provide limited metrics of model performance. Cryo. 8, 229–243. (doi:10.5194/tc-8-229-2014), 2014.

Notz, D.: How well must climate models agree with observations?, Philosophical Transactions of the Royal Society of London A: Mathematical, Phys. and Engin. Sci., 373, https://doi.org/10.1098/rsta.2014.0164, 2015.

Ohshima, K. I., Nihashi, S., and Iwamoto, K.: Global view of sea-ice production in polynyas and its linkage to dense/bottom water formation, Geoscience Letters, 3, 13, 2016.

O'Reilly, J. E., Maritorena, S., Mitchell, B. G., Siegel, D. A., Carder, K. L., Garver, S. A., Kahru, M. and McClain, C.: Ocean color chlorophyll algorithms for SeaWiFS, J. Geophys. Res., 103, 24,937– 24,953, 1998.

OSI SAF Global sea ice concentration climate data record 1978-2020 (v3.0, 2022), OSI-450-a, doi:10.15770/EUM_SAF_OSI_0013. EUMETSAT Ocean and Sea Ice Satellite Application Facility. Data extracted from E. U. Copernicus Marine Service Information: accessed 23 January, 2025.

Parkinson, C. L. and Cavalieri, D. J.: Antarctic sea ice variability and trends, 1979–2010, The Cryo., 6, 871–880, https://doi.org/10.5194/tc-6-871-2012, 2012.

Parkinson, C., and Cavalieri, D.: Antarctic sea ice variability and trends, 1979–2010. *The Cryosphere*, **6**, 871–880, 2012.

Parkinson, C. L.: A 40-y record reveals gradual Antarctic sea ice increases followed by decreases at rates far exceeding the rates seen in the Arctic, P. Natl. Acad. Sci. USA, 116, 14414–14423, 2019.

Purich, A., and Doddridge, E. W.: Record low Antarctic sea ice coverage indicates a new sea ice state. Commun Earth Environ 4, 314. https://doi.org/10.1038/s43247-023-00961-9, 2023.

Raphael, M.N., and Handcock, M. S.: A new record minimum for Antarctic sea ice. Nat Rev Earth Environ 3, 215–216. https://doi.org/10.1038/s43017-022-00281-0, 2022.

Richert, I., Yager, P., Dinasquet, J., Logares, R., Riemann, L., Wendeberg, A., Bertilsson, S. and D. Scofield, D.: Summer comes to the Southern Ocean: how phytoplankton shape bacterioplankton communities far into the deep dark sea. Ecosphere. 10. e02641. 10.1002/ecs2.2641, 2019.

Roach, L. A., Dörr, J., Holmes, C. R., Massonnet, F., Blockley, E. W., Notz, D., et al. (2020). Antarctic sea ice area in CMIP6. Geophysical Research Letters, 47, e2019GL086729. https://doi.org/10.1029/2019GL086729

Rodgers, K. B., Lee, S.-S., Rosenbloom, N., Timmermann, A., Danabasoglu, G., Deser, C., Edwards, J., Kim, J.-E., Simpson, I. R., Stein, K., Stuecker, M. F., Yamaguchi, R., Bódai, T., Chung, E.-S., Huang, L., Kim, W. M., Lamarque, J.-F., Lombardozzi, D. L., Wieder, W. R., and Yeager, S. G.: Ubiquity of human-induced changes in climate variability, Earth Syst. Dynam., 12, 1393–1411, https://doi.org/10.5194/esd-12-1393-2021, 2021.

Singh, H. K. A., Landrum, L., Holland, M. M., Bailey, D. A. and A. K. DuVivier, A. K.: An overview of Antarctic sea ice in the CESM2: analysis of the seasonal cycle, predictability, and atmosphere-ocean-ice interactions. J Adv Model Earth Syst., 13, https://doi.org/10.1029/2020MS002143, 2020.

Smith, A., Jahn, A., and Wang, M.: Seasonal transition dates can reveal biases in Arctic sea ice simulations, The Cryosphere, 14, 2977–2997, https://doi.org/10.5194/tc-14-2977-2020, 2020.

Smith, A., Jahn, A., Burgard, C., and Notz, D.: Improving model-satellite comparisons of sea ice melt onset with a satellite simulator, The Cryosphere, 16, 3235–3248, https://doi.org/10.5194/tc-16-3235-2022, 2022.

Stammerjohn, S. E., Martinson, D. G., Smith, R. C., Yuan, X. and Rind, D.: Trends in Antarctic annual sea ice retreat and advance and their relation to El Nin˜o–Southern Oscillation and Southern Annular Mode variability, J. Geophys. Res., 113, C03S90, doi:10.1029/2007JC004269, 2008.

Tamura, T., Ohshima, K. I., Enomoto, H., Tateyama, K., Muto, A., Ushio, S. and R. A. Massom, R. A.: Estimation of thin sea-ice thickness from NOAA AVHRR data in a polynya off the Wilkes Land coast, East Antarctica. Ann. Glaciol., 44, 269–274, 2006.

Tamura, T., Ohshima, K. I., Markus, T., Cavalieri, D. J., Nihashi, S. and N. Hirasawa, N.: Estimation of thin ice thickness and detection of fast ice from SSM/I data in the Antarctic Ocean, J. Atmos. Oceanic Technol., 24, 1757– 1772, 2007.

Tamura, T., Ohshima, K. I., and Nihashi, S.: Mapping of sea ice production for Antarctic coastal polynyas. Geophys Res Lett 35:L07606, 2008.

Tamura, T., Ohshima, K. I., Fraser, A. D. and G. D. Williams, G. D.: Sea ice production variability in Antarctic coastal polynyas, J. Geophys. Res. Oceans, 121, 2967–2979, doi:10.1002/2015JC011537, 2016.

Thompson, L., Smith, M., Thomson, J., Stammerjohn, S., Ackley, S., and Loose, B.: Frazil ice growth and production during katabatic wind events in the Ross Sea, Antarctica, The Cryosphere, 14, 3329–3347, https://doi.org/10.5194/tc-14-3329-2020, 2020.

Tsujino, H., Urakawa, S., Nakano, H., Small, R. J., Kim, W. M., Yeager, S. G., Danabasoglu, G., Suzuki, T., Bamber, J. L., Bentsen, M., B¨oning, C. W., Bozec, A., Chassignet, E. P., Curchitser, E., Boeira Dias, F., Durack, P. J., Griffies, S. M., Harada, Y., Ilicak, M., Josey, S. A., Kobayashi, C., Kobayashi, S., Komuro, Y., Large, W. G., Le Sommer, J., Marsland, S. J., Masina, S., Scheinert, M., Tomita, H., Valdivieso, M., and Yamazaki, D.: Jra-55 based surface dataset for driving ocean–sea-ice models (jra55-do). Ocean Modelling, **130**:79–139, 2018.

Turner, J., Phillips, T., Marshall, G. J., Hosking, J. S., Pope, J. O., Bracegirdle, T. J., and Deb, P.: Unprecedented springtime retreat of Antarctic sea ice in 2016, Geophys. Res. Lett., 44, 6868–6875, 2017.

Turner, J., Holmes, C., Caton Harrison, T., Phillips, T., Jena, B., Reeves-Francois, T., Fogt, R., Thomas, E. R., and Bajish, C. C.: Record low Antarctic sea ice cover in February 2022. Geophys. Res. Lett., 49, e2022GL098904, 2022.

Windnagel, A., Meier, W., Stewart, S., Fetterer, F., & Stafford, T.: NOAA/NSIDC Climate Data Record of Passive Microwave Sea Ice Concentration Version 4 Analysis. NSIDC Special Report 20. Boulder CO, USA: National Snow and Ice Data Center, 2021.

Zygmuntowska, M., Rampal, P., Ivanova, N. and L. H. Smedsrud, L. H.: Uncertainties in Arctic sea ice thickness and volume: new estimates and implications for trends, The Cryosphere, 8 (2), 705–720, doi:10.5194/tc-8-705-2014, 2014.